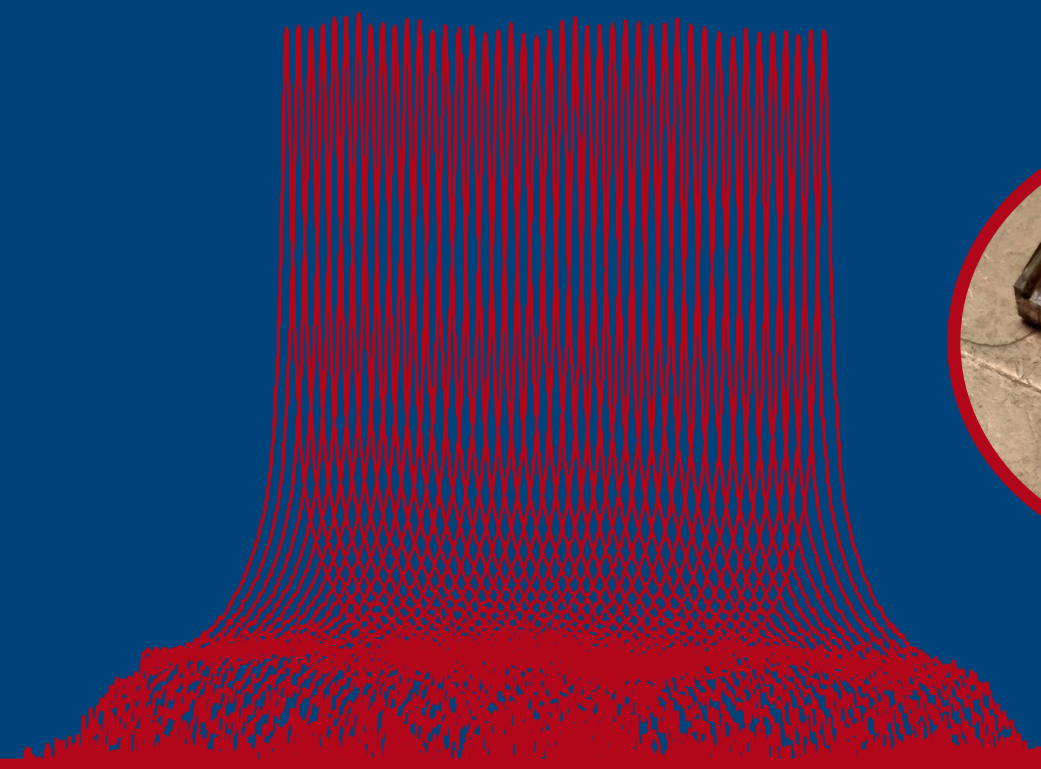


Continuous wavelength tuning of an integrated extended-cavity laser beyond its mode spacing limit

Albert van Rees



Continuous wavelength tuning of an integrated extended-cavity laser beyond its mode spacing limit

Albert van Rees

Master's Thesis

Applied Physics, University of Twente

Enschede, July 2019

Daily supervisors:

Dr. Y. Fan

Dr. P.J.M. van der Slot

Graduation committee:

Prof. dr. K.-J. Boller

Dr. P.J.M. van der Slot

Dr. ir. H.L. Offerhaus

Dr. ir. D. Geskus

This work was done at:

Laser Physics and Nonlinear Optics (LPNO)

Mesa+ Institute for Nanotechnology

Faculty of Science and Technology (TNW)

University of Twente

P.O. Box 217

7500 AE Enschede, the Netherlands

This project has received funding from the European Union's Horizon 2020 research and innovation programme under grant agreement No 780502 (3PEAT).

Acknowledgements

After a prolonged journey through my study of applied physics, I am both grateful and happy that with this thesis I can finally end my MSc. During this journey, many people encouraged and convinced me not to give up and to arrive at this finish. Without their support, I would not have arrived here. One important path throughout this journey was to work in the field of photonics, first at XiO Photonics, and later at LioniX International, for more than 8 years in total. With my work there, designing and characterizing photonic chips, I regained my motivation for physics and started to enjoy integrated photonics. I would like to thank again my former colleagues, in particular, Edwin, Ronald, Douwe, René and Hans, for providing me that opportunity.

Through the collaboration between LioniX and LPNO, I met Klaus Boller, who convinced me to do this MSc assignment in the LPNO group on the subject of hybrid lasers. Klaus, thank you for having faith in me and encouraging me to push my limits. It is always a pleasure to listen to your clear explanations with humorous examples. Therefore, I will continue this work with confidence as a PhD student in this group.

I thank Youwen Fan for being my daily supervisor at the start of this assignment and for transferring your enthusiasm for the hybrid lasers to me. It is an honor for me to continue where you left off. Peter van der Slot, many thanks for the time and effort to guide me through writing this thesis. The discussions about the outcomes of measurements and your emphasis on correct formulation made this work a lot better. Jesse, I learned a lot from you, starting with all the things I needed to know for working in this group, to the many talks we had about fit methods and measurement results. Thank you for the countless liters of free coffee from the machine at the corridor! Caterina, the ‘queen’ of LPNO, I admire your effort to convince me to participate in the dance workshop, even if only as a photographer. Thank you very much for your encouragement with my first talk at the ANP retreat, that made the difference!

During my own assignment I was allowed to supervise Rob, Lida and Kees with their assignments. I enjoyed it to discuss the lasers with you and to perform several measurements together. Sharing the knowledge is very useful for understanding what matters. Thank you all for dealing with me, for example when I didn’t have time because I had to finish this report.

I also thank the rest of the group for the pleasant place to work, the conversations and the jokes during the lunch and coffee breaks. Thank you: Bas, Bert, Carla, David, Haider, Maarten, Okky, Robert, Roel, Tara, Victoria, Xin and Yvan.

This work would never have been possible without the input from many of my former LioniX colleagues. Dimitri, thank you for the assembly of the laser and starting the plenary discussion about mode-hop-free tuning. Ruud, thank you for your contribution to the design of these lasers and the suggestion for simultaneous tuning. Marcel, thank you for the mask design and providing all the relevant data. Edwin, the elegant electronics you designed were crucial for operating the lasers and obtaining these results. Araldo, thank you for your contribution to the electronics and providing an upgrade to the DAC controllers. Jörn and Erik, it was a pleasure to attend the 3PEAT meetings with you. Robert, thanks for arranging the Finisar OSA for the high-resolution measurements. René and Hans, thank you for providing the opportunity for filing a provisional patent application. I probably forgot to mention some more names, because many people are involved in the development, fabrication and assembly of these lasers.

I would like to thank Herman Offerhaus and Dimitri Geskus for taking part in the graduation committee as external members.

Finally, I am very grateful to my friends and family who always supported me throughout my study. Marko, thank you for your friendship and support. It was an honor to be a paranymp at your PhD defense. Papa, mama en Maria, bedankt voor jullie steun in zowel de moeilijke als de succesvolle jaren van mijn studie!

Albert van Rees

Enschede, Juli 2019

Abstract

Chip-sized diode lasers having both an ultra-narrow linewidth and a large continuous wavelength tuning range are of high interest for many applications. Ultra-narrow intrinsic laser linewidths can be obtained by hybrid integration of a semiconductor amplifier with a low-loss dielectric waveguide-based feedback circuit. This integrated extended-cavity provides spectrally-selective feedback and a significant extension of the cavity length, which narrows the laser linewidth. However, as the length of the laser cavity increases, the cavity mode spacing decreases, which causes undesired instabilities in the form of mode hops when tuning the laser wavelength. We overcome these instabilities and experimentally demonstrate a new approach towards mode-hop-free tuning of such lasers, well beyond the standard limit that is formed by the cavity mode spacing. This approach addresses the conflicting demands on the laser cavity length resulting from the requirement of both a narrow intrinsic linewidth and a large continuous tuning range. Furthermore, we present for the first time an analytical model that describes the mode-hop-free tuning as realized with this approach. After calibration, this model can be used to accurately predict the laser wavelength anywhere within its mode-hop-free tuning range. We demonstrate this by measuring several absorption lines of acetylene with a high accuracy and resolution.

The hybrid laser used in the experiments comprises an InP amplifier and a Si_3N_4 waveguide feedback circuit with a tunable phase section, and a Vernier filter comprising two tunable microring resonators of slightly different radii. When tuning the laser by tuning the phase section only, this results in mode-hop-free tuning only over a single free spectral range of the laser cavity, which is 0.034 nm. To overcome this tuning limit, we synchronously control the phase section and both rings with a proper ratio, resulting in a mode-hop-free tuning range increase by a factor of 6 to 0.22 nm. This increase is not only due to the synchronization of the three involved tuning elements. In addition, the synchronous tuning results in a 2.8 times larger tuning slope of the laser wavelength versus phase section heater power, which corresponds to much shorter laser cavity where the rings are not present.

These results indicate that both an ultra-narrow linewidth and a broad mode-hop-free tuning range can be achieved with a fully integrated extended-cavity laser based on microring resonators.

Contents

Acknowledgements.....	iv
Abstract.....	vi
1 Introduction.....	1
2 Theoretical background.....	5
2.1 Optical waveguides.....	5
2.2 Wavelength tuning.....	6
2.3 Laser cavity and phase section.....	7
2.4 Microring resonator.....	9
2.5 Vernier filter.....	12
2.6 Mode-hop-free tuning.....	13
3 Laser device and set-up.....	17
3.1 Hybrid integrated laser.....	17
3.2 Butterfly package and PCB.....	19
3.3 Experimental set-up.....	20
4 Experimental results.....	23
4.1 Laser characteristics.....	23
4.2 Laser tuning response.....	26
4.2.1 Heater resistances.....	26
4.2.2 Tuning by the phase section.....	27
4.2.3 Tuning by a single microring resonator.....	28
4.3 Mode-hop-free tuning.....	31
4.4 Acetylene absorption spectroscopy with mode-hop-free laser tuning.....	33
4.4.1 Acetylene absorption spectrum.....	33
4.4.2 Wavelength sweep over an acetylene absorption line.....	34
5 Conclusions and outlook.....	37
6 References.....	39
7 List of publications.....	42
Appendix A.....	43
A.1 Laser cavity free spectral range.....	43
A.2 Laser cavity resonant wavelength tuning.....	44
A.3 Microring resonator effective length.....	45

1 Introduction

Light is an essential ingredient for our lives. It allows to observe the world we live in, it plays a central role in photosynthesis and, for example, it is at the foundation of our modern information society. Most of the light around us is based on the process of spontaneous emission, which is a random event in which a system decays from an excited energy state to a lower energy state by emission of a light particle known as a photon.

In the 1960s a new type of light source, the laser¹, was invented^[2], which was based on stimulated emission, a process already predicted by Einstein^[3]. In this process, an appropriate photon stimulates an atom in an excited state to decay to a lower energy state by emitting a photon with the same properties as the incident photon, which leads to coherent amplification of the light. The invention of the laser heralded a new era of novel light sources with special capabilities. These unique capabilities, *e.g.*, high spatial and temporal coherence, large choice of wavelengths and high radiance quickly led to a huge variety of applications. Nowadays, these applications range from various forms of material processing and manufacturing to numerous medical applications to sensing and security applications to high-precision metrology to high-speed, high-bandwidth optical data transmission and many more.

The gain medium of a laser, where the light is amplified, can be formed of many different material types, *e.g.*, the first laser used a ruby crystal^[2]. Shortly after the introduction of the first laser, lasers were developed based on semiconductor materials^[4]. Currently, the semiconductor-based laser diode is the most used and widespread laser type. The small size, low cost, direct electric pumping and high efficiency makes these devices very suitable for integration in many systems. In addition, the advance of integrated optics gives the semiconductor laser an even more central role, because these lasers can be integrated as light sources into photonic integrated circuits.

The increasing demand for data speed and bandwidth by our information society drives the need for robust and compact light sources that can be continuously tuned and have a narrow intrinsic linewidth. For example, in the field of coherent optical communication, an ultra-narrow intrinsic linewidth is required for data transmission over optical fiber links, using higher order modulation formats, such as 4096-QAM^[5]. On the other hand, increasing the capacity of optical fiber links by dense wavelength division multiplexing (WDM) requires the laser wavelength to be tuned to a specific channel in a frequency grid^[6] and to electronically stabilize it to that channel. Other fields that greatly benefit from narrow-linewidth tunable lasers are, amongst others, high-resolution spectroscopy^[7] using fully integrated^[8] dual Kerr frequency combs^[9], optical sensing^[10] for lab-on-a-chip applications^[11], interferometry^[12], integrated photonic clocks^[13] and microwave photonic links^[14].

Basic laser theory shows that the continuous tuning range for a standard semiconductor Fabry-Pérot laser is limited by the free spectral range of the laser cavity, which is inversely proportional to its optical length^[15]. On the other hand, the linewidth of the laser is determined by the frequency (or phase) fluctuations. These fluctuations are ultimately limited by spontaneous emission via the so-called Schawlow-Townes limit^[16], which scales with the reciprocal of the length of the laser cavity squared. Increasing the cavity length will reduce the laser linewidth, because this reduces the number of spontaneous emission photons in the lasing mode with respect to the stimulated emission photons. Reducing technical noise contributions to the linewidth is typically easier for lasers with a small Schawlow-Townes linewidth, by using feedback loops and, *e.g.*, lock the laser frequency to an external reference. Stabilization and locking of the laser also requires continuous tuning^[17] as a sudden and discontinuous jump of the laser wavelength is hard to correct in a servo control system.

¹ Actually, the maser was demonstrated a few years earlier and also relied on the process of stimulated emission to produce coherent electromagnetic radiation in the microwave spectral range^[1].

These considerations, unfortunately, show that requiring both a large continuous wavelength tuning range and a small Schawlow-Townes linewidth results in conflicting demands on the laser cavity length. A large tuning range requires a short cavity length, while a small Schawlow-Townes linewidth requires a long cavity length. Typical diode lasers, such as distributed Bragg reflector (DBR) and distributed feedback (DFB) lasers, either have a short cavity length, below a few hundred micrometer, with an associated large tuning range and a broad linewidth in the MHz-range, or have a long cavity length with an associated small tuning range and a narrow linewidth. As the length of the laser cavity increases, the free spectral range of the laser cavity, which limits the continuous tuning range, decreases.

The conflicting demands on the laser cavity length resulting from the requirement of both a large continuous tuning range and a narrow Schawlow-Townes linewidth have been addressed in several ways. Here, we recall solutions applied to diode lasers. Typically, one facet of the diode laser is anti-reflection coated and, using bulk optics, an extended cavity is created for the diode laser which can be substantially longer. An appropriately narrow spectral filter is added inside the laser cavity to select a single cavity mode. When tuning such a laser by changing the cavity length, the filter has to be tuned synchronously, in order to avoid undesired mode hops, which result in discontinuous wavelength changes. For example, in a bulk external cavity laser, continuous tuning was demonstrated using a grating as filter in both a Littman-Metcalf^[18] and Littrow configuration^[19]. More recently, continuous tuning of an external cavity laser has been reported by synchronous rotation of a multi-layered dielectric filter with extension of the cavity^[20]. Although continuous tuning is possible ultimately over the full gain bandwidth, these bulk external cavity lasers are intrinsically sensitive to mechanical vibration and misalignments.

To provide a fundamentally more stable solution, we investigate in this thesis a fully integrated extended cavity to obtain single mode lasing of a semiconductor laser with a large tuning range combined with a narrow Schawlow-Townes linewidth. This solution allows for easy system integration at low cost, which would make more applications economically feasible.

Liu *et al.* proposed a microring resonator (MRR) coupled diode laser to obtain single mode lasing with a narrow Schawlow-Townes linewidth^[21]. The filtering mechanism of a microring resonator provides a very sharp Lorentzian shaped transmission peak, to select a single laser mode, and it effectively extends the on-chip optical cavity length of the laser. To provide a low-loss feedback circuit for the diode laser, bending losses will limit the workable ring radius, and thus limit the free spectral range of the filter. However, by using a combination of two or more microring resonators as filter, a free spectral range of the filter equal to or surpassing the gain bandwidth can be obtained via the so-called Vernier effect^{[21], [22]}, thereby allowing single mode and narrow linewidth operation over the complete gain bandwidth of the diode laser. For example, by integrating two ring resonators on a low loss feedback circuit and coupling this circuit with a semiconductor optical amplifier, the linewidth can be reduced to the 10-kHz-range^{[23]-[25]}. Recently, an extremely narrow linewidth of 290 Hz has been reported, by adding a third ring resonator^[26].

When multiple rings are used as a single mode filter, different laser architectures are possible. The effect of different architectures on laser performance has been investigated by Komljenovic *et al.*, with the so-called ring-bus-ring architecture having the most promising performance^[27]. All architectures investigated have separate tuning of a phase section to change the cavity phase and tuning of the microrings to shift its resonances, although using a single tuning element has been proposed^[28]. Wide-tuning of these devices, *i.e.*, covering the complete gain bandwidth, has widely been demonstrated^{[23]-[25]}. However, mode-hop-free tuning of these lasers has not been studied so far.

The laser used for studying mode-hop-free tuning in this thesis is schematically shown in Fig. 1.1. The laser comprises a semiconductor (InP) chip and a glass ($\text{Si}_3\text{N}_4/\text{SiO}_2$) chip. The semiconductor chip contains an optical amplifier and a feedback mirror in the form of a high reflectivity (HR)

coating on one facet of the chip. The low-loss dielectric glass chip implements a phase section and two sequential microring resonators, placed inside a loop mirror, following the bus-ring-bus architecture^[27]. This combination allows for wavelength selective feedback. Further, a balanced Mach-Zehnder interferometer, used as a tunable coupler, extracts part of the resonating light towards the output port of the integrated laser, which is butt-coupled to an output fiber. This particular feedback configuration allows tuning over the full gain bandwidth of the amplifier and imposes a narrow Schawlow-Townes laser linewidth in the 10-kHz range. Full electronic tuning is realized via five resistive heaters that are placed above the phase section, the two microrings (MRR1 and MRR2) and the tunable coupler (two heaters, one above each arm), respectively. By applying an electric current to the heaters, the material refractive index and thus the optical length of these sections can be controlled, *i.e.*, the phase of the light passing through each section.

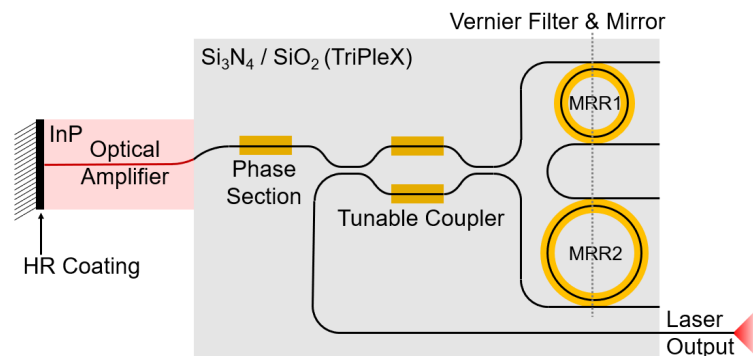


Fig. 1.1: Schematic view of the integrated laser. Shown are the semiconductor optical amplifier with a high reflectivity coating on one facet, the phase section, the two sequential microring resonators in a loop mirror to provide wavelength selective feedback, and a tunable coupler to direct part of the light to the output port of the laser. The output of the laser is available via a fiber that is butt-coupled to the output port.

Using microrings for the spectral filtering has the added advantage that a small change to the optical length of one of the rings, *i.e.*, a small change in phase advance acquired during one roundtrip, is enhanced with respect to a single roundtrip, because the lifetime of the light inside the ring is much larger than one roundtrip time. In this thesis, we present for the first time a theoretical analysis for mode-hop-free tuning based on this effect and we confirm the analysis with experimental data. The analysis shows that the tuning sensitivity, *i.e.*, the change in lasing wavelength with a change in optical phase induced by the phase section, is that of the same laser without the microrings. This means that the tuning sensitivity corresponds to that of a laser having a short laser cavity without microrings, while the Schawlow-Townes linewidth corresponds to that of a laser having a long laser cavity with microrings.

This thesis is organized as follows. In chapter 2 we briefly recall the appropriate theory for waveguiding of light and develop an analytic model that describes mode-hop-free tuning. The hybrid laser used in the experiment and the experimental setup is described in chapter 3. Chapter 4 describes for the first-time experimental results for on-chip, all-electronic and mode-hop-free tuning of such a laser, with a tuning range that extends beyond its mode spacing limit. Finally, in chapter 5, a summary of the results is presented together with a conclusion and outlook.

2 Theoretical background

Here we present a model for the wavelength tuning of the hybrid laser. A first goal is finding analytical expressions that describe the tuning behavior and can be compared with experimental data for validation. The second goal is to use the expressions for drawing conclusions on the general requirements for continuous tuning. The third goal is to investigate the potential for further extension of the tuning range. We present only the most important steps of the derivation, while a detailed derivation is found in appendix A.

2.1 Optical waveguides

Optical waveguides are the fundamental elements of integrated photonics, to guide light within photonic chips and interconnect the different building blocks of a photonic integrated circuit. A waveguide is a structure to guide an electromagnetic wave along the waveguide axis, while restricting the propagation into the other directions. This allows electromagnetic waves to be confined to a small area without the divergence as found in diffraction in free space. The physical background of a waveguide can be found in more detail in several textbooks^{[29]–[31]}.

For a typical dielectric waveguide, the confinement of the light is based on total internal reflection. This happens when a dielectric material of higher refractive index surrounded by materials of lower refractive index. The cross-section of an optical waveguide can have different geometries, but the material with the highest refractive index always forms the core of the waveguide. Based on the refractive index contrast, the shape and size of the waveguide, one or more transverse optical modes can be guided by the waveguide at a specific wavelength. These spatial patterns of the electromagnetic field are discrete solutions to the Maxwell equations for the specific waveguide structure.

Each transverse optical mode can be characterized by its propagation constant, given by

$$\beta = k_0 n_{\text{eff}}(\lambda) = \frac{2\pi}{\lambda} n_{\text{eff}}(\lambda), \quad (2.1)$$

where k_0 is the wave vector of light in vacuum, λ is the vacuum wavelength and n_{eff} is the effective refractive index of the mode. This effective refractive index can be understood as a weighted average of the refractive indices of the involved materials, weighted by the fraction of the electromagnetic field in each material. The effective refractive index of the transverse optical mode is wavelength dependent as a result of chromatic dispersion of the involved dielectric materials and due to form dispersion, which is the wavelength dependence of the optical mode on the waveguide cross section. To obtain an approximate estimate of the value for a rectangular waveguide, analytical methods are available^[32]. However, for gaining higher precision and due to the universality of the approach, it is more customary to use numerical mode solvers.

If only one fundamental mode is supported by an optical waveguide per polarization direction, the waveguide is called ‘single-mode’. The advantage of supporting only a single mode is that both the spatial distribution and the propagation of the electromagnetic wave are predictable, such that the optical functionality of building blocks based on these single mode waveguides remains reliable.

When multiple wavelengths propagate through a dispersive medium, such as an optical waveguide, they form a propagating beat pattern. The propagation delay of this beat pattern is quantified by the group index, n_g , which can be derived from the effective refractive index via^[29]

$$n_g(\lambda) = n_{\text{eff}}(\lambda) - \lambda \frac{dn_{\text{eff}}(\lambda)}{d\lambda}. \quad (2.2)$$

2.2 Wavelength tuning

The hybrid laser we consider here has been introduced in chapter 1 and consists of an InP semiconductor optical amplifier (SOA) connected to a wavelength-tunable feedback circuit implemented using Si_3N_4 waveguides (see Fig. 1.1). Tuning of the wavelength at which the laser oscillates can be done by tuning of the phase section as well as tuning of the microring resonators present in the feedback circuit via resistive heaters placed on top of these elements.

In order to model the tuning of the laser and how the heaters modify the laser wavelength, the effect of a heater on the propagating mode must be known. The basic physical effect of the heater on the propagating mode is well understood, namely that the heaters change the refractive index of the core and cladding materials, Si_3N_4 and SiO_2 , respectively, which changes the effective index of the guided optical mode, while the physical length change can be neglected. The changes in the refractive indices are sufficiently small such that the transverse field distribution is unaffected by the heaters. The effect of the heaters is thus mainly a change in optical phase of the guided mode. The electric-thermal-optical performance can be well modeled using finite-element modelling, and therefore, a well-defined change in optical phase can be determined. Even if there is a small uncertainty in material properties due to fabrication uncertainties, all the heaters can still be calibrated. Therefore, we assume that the sole action of each heater element is to modify the optical phase by an amount ϕ_{ps} , ϕ_{r1} or ϕ_{r2} for the cavity phase section (PS) and the microrings MRR1 and MRR2, respectively. For the hybrid semiconductor-glass laser investigated here, the maximum change in optical phase is about 2.5π for the 1-mm-long phase section used and 1.5π for the ring resonators. This maximum phase shift is limited by the maximum dissipated electrical power without breakdown of the heaters, which is determined by the material properties and physical dimensions of the heaters.

The tuning of the laser cavity can either be described in the frequency or wavelength domain. Here we make the arbitrary choice to describe the tuning in the wavelength domain. To find the tuning sensitivity $\frac{\partial \lambda}{\partial \phi}$ for the laser, *i.e.*, the change in laser wavelength $\Delta \lambda = \frac{\partial \lambda}{\partial \phi} \Delta \phi$ when the optical phase of the light changes by a small amount $\Delta \phi$, we need to consider the tuning sensitivities due to the PS, MRR1 and MRR2. This involves determining the tuning sensitivity $\frac{\partial \lambda_{\text{r1}}}{\partial \phi_{\text{r1}}}$ and $\frac{\partial \lambda_{\text{r2}}}{\partial \phi_{\text{r2}}}$ for resonant wavelength λ_{r1} and λ_{r2} for the two microrings MRR1 and MRR2, respectively. This also involves determining the tuning sensitivity of the laser wavelength, λ_c , by tuning the phase section alone, $\frac{\partial \lambda_c}{\partial \phi_{\text{ps}}}$, and the tuning sensitivity $\frac{\partial \lambda_c}{\partial \phi_{\text{r1}}}$ and $\frac{\partial \lambda_c}{\partial \phi_{\text{r2}}}$ of the laser wavelength when tuning the microrings separately for the two microrings MRR1 and MRR2, respectively. Finally, the tuning sensitivity $\left(\frac{\partial \lambda_c}{\partial \phi_{\text{ps}}}\right)_{\text{MHF}}$ of the laser wavelength by the phase section with synchronous tuning of the two microring resonators, *i.e.*, in the case of mode-hop-free tuning, will be determined.

These tuning sensitivities are connected to the free spectral ranges $\Delta \lambda_c$, $\Delta \lambda_{\text{r1}}$ and $\Delta \lambda_{\text{r2}}$ of the laser cavity and the microrings MRR1 and MRR2, respectively, as follows. When the wavelength changes over one free spectral range, the optical phase increases in all cases by 2π . In addition, we will relate these free spectral ranges with the effective lengths $L_{\text{eff},c}$, $L_{\text{eff},\text{r1}}$ and $L_{\text{eff},\text{r2}}$ of the laser cavity and the microrings, to connect the tuning sensitivities with the physical dimensions and design specifications of the laser.

To simplify the analysis, the derivation of the laser wavelength tuning is carried out for the case of a so-called cold-cavity, *i.e.*, a laser cavity without any gain present. Furthermore, we are primarily interested here in the tuning of the laser wavelength and not in its absolute value. Including gain would shift the resonances of the laser cavity, *e.g.* via frequency pulling by the frequency dependent

gain and via gain-index coupling in the semiconductor material. However, including gain at a fixed value, *i.e.*, fixed injection current, would have limited to no effect on the tuning via the heaters.

2.3 Laser cavity and phase section

To describe the tuning of the laser cavity under consideration, we start with analyzing the cold-cavity resonances. These resonances are found when the cold-cavity roundtrip phase, $\theta_{rt,c}$ fulfills the resonance condition

$$\theta_{rt,c} = m_c 2\pi, \quad (2.3)$$

where m_c is an integer, which indicates the number of wavelengths that fit along one roundtrip of the laser cavity, also called the cavity mode number. The actual value of the integer is determined by the wavelength that is closest to where the laser shows the highest ratio of roundtrip gain to roundtrip loss. This ratio is usually highest at the peak of the laser's gain spectrum, unless intra-cavity filters are inserted to give a different spectral region a higher ratio of gain and loss. At non-integer multiples of the mode number, due to destructive interference in multiple roundtrips, the light intensity in the amplifier will be less, rendering a reduced or even zero stimulated emission rate.

The cavity roundtrip phase is determined by the local propagation constant of the light integrated over the distance propagated. The distance the light effectively propagates through the microring is defined as $L_{eff,r1}$ and $L_{eff,r2}$ for MRR1 and MRR2, respectively. Then, the cold-cavity roundtrip phase is given by

$$\theta_{rt,c} = 2L_{SOA}\beta_{SOA} + 2L_{bus}\beta_{Si_3N_4} + L_{eff,r1}\beta_{Si_3N_4} + L_{eff,r2}\beta_{Si_3N_4}, \quad (2.4)$$

where β_i is the local propagation constant, as defined in Eq. 2.1, in section i ($i = SOA$ or Si_3N_4). Note, that both the propagation constants as well as the effective lengths of the microring resonators are wavelength dependent. $2L_{SOA}$ is the geometrical roundtrip length of the semiconductor optical amplifier (SOA), and $2L_{bus}$ is the geometrical roundtrip length of Si_3N_4 bus waveguides belonging to the laser cavity excluding the microrings. The microring effective lengths are not multiplied by 2, because these microrings are part of the loop mirror that forms one of the end mirrors of the laser cavity. Note that

$$\beta_{SOA} = \beta_{Si_3N_4} \frac{n_{eff,SOA}}{n_{eff,Si_3N_4}}, \quad (2.5)$$

and by defining $\beta \equiv \beta_{Si_3N_4}$ and using Eq. 2.5 we can rewrite Eq. 2.4 as

$$\theta_{rt,c} = 2L_{eff,c}\beta, \quad (2.6)$$

where we have introduced the effective cavity length $L_{eff,c}$ as

$$L_{eff,c} = \frac{n_{eff,SOA}}{n_{eff,Si_3N_4}} L_{SOA} + L_{bus} + \frac{1}{2}(L_{eff,r1} + L_{eff,r2}). \quad (2.7)$$

The weight factor $\frac{n_{eff,SOA}}{n_{eff,Si_3N_4}}$ is included here because the light propagates at a higher speed through the dielectric waveguides as compared to the semiconductor waveguide, due to the differences in effective index.

To make the dependence of the cold-cavity roundtrip phase $\theta_{rt,c}$ on the vacuum wavelength λ more explicit, we rewrite Eq. 2.6 by using Eq. 2.1 as

$$\theta_{rt,c} = \frac{4\pi L_{eff,c}(\lambda) n_{eff}(\lambda)}{\lambda} \quad (2.8)$$

where we have introduced $n_{\text{eff}} \equiv n_{\text{eff},\text{Si}_3\text{N}_4}$ and made the wavelength dependence of the effective cavity length explicit. We further write the effective refractive index explicitly as $n_{\text{eff}}(\lambda)$ to express that it depends on the wavelength as a result of both chromatic dispersion of the involved dielectric materials as well as due to the geometry of the waveguide. The effective cavity length $L_{\text{eff},c}(\lambda)$ has a strong wavelength dependence because the effective length of the microring resonators is strongly wavelength dependent, becoming much larger than the geometrical circumference of the rings near the resonances of the rings, as will be described in more detail section 2.4.

Starting from Eq. 2.8, and by imposing the resonance condition for the roundtrip phase, the longitudinal mode spacing of the laser cavity can be derived. This spacing, defined as the wavelength difference between two subsequent resonant modes of the laser cavity, is also called the cavity free spectral range (FSR). The FSR, $\Delta\lambda_c$, is given by (see appendix A.1 for the derivation)

$$\Delta\lambda_c = \frac{\lambda_c^2}{2n_g(\lambda_c)L'_{\text{eff},c}(\lambda_c)}, \quad (2.9)$$

where λ_c^2 is the vacuum wavelength of the cavity belonging to resonant mode m_c . $L'_{\text{eff},c}$ is nearly the same as $L_{\text{eff},c}$ introduced in Eq. 2.7 but with the ratio $\frac{n_{\text{eff},\text{SOA}}}{n_{\text{eff},\text{Si}_3\text{N}_4}}$ replaced by $\frac{n_{g,\text{SOA}}}{n_{g,\text{Si}_3\text{N}_4}}$ and $n_{g,\text{Si}_3\text{N}_4} \equiv n_g$.

It is interesting to note that the group index, n_g , appears in Eq. 2.9, although our derivation did not intend to describe the propagation of multiple wavelengths in the laser cavity, as we aim solely on describing single-wavelength oscillation. Nevertheless, describing the distance between the resonant cavity modes requires to calculate the resonator properties at two subsequent resonant wavelengths, separated by one FSR, which is why the group index enters the equation.

Tuning of the cavity resonant wavelength via the phase section can be modeled by including the single-pass phase, ϕ_{ps} , added by the phase section, to Eq. 2.8,

$$\theta_{\text{rt},c} = \frac{4\pi L_{\text{eff},c}(\lambda_c)n_{\text{eff}}(\lambda_c)}{\lambda_c} + 2\phi_{ps}, \quad (2.10)$$

where the factor 2 is due to the fact that the light passes the phase section twice during one laser cavity roundtrip. In appendix A.2 is shown that Eq. 2.10 leads to a tuning slope, $\frac{\partial\lambda_c}{\partial\phi_{ps}}$, of the cavity resonant wavelength given by

$$\frac{\partial\lambda_c}{\partial\phi_{ps}} = \frac{\Delta\lambda_c}{\pi} \quad (2.11)$$

Equation 2.11 reveals that the tuning sensitivity for tuning the phase section is simply determined by the free spectral range of the laser cavity. For instance, multiplying Eq. 2.11 with a phase shift of almost π , increases the wavelength of the considered mode by almost one FSR, which is to be expected as the roundtrip optical phase advance is then almost 2π and this is the optical phase difference for two adjacent longitudinal modes of the resonator.

However, if a phase shift larger than π is applied, the wavelength of the considered mode (m_c) tunes farther than one FSR away from the original wavelength. This means that now the neighboring mode with order $m_c + 1$ (or $m_c - 1$) is closer to the wavelength of optimum gain-to-loss ratio. In this case, laser oscillation will start up at that neighboring mode, which ceases oscillation of the former mode via gain competition, which is well-known as a mode hop². These hops form the standard limit to mode-hop-free tuning of any laser. Solely tuning the phase section does not allow a wider continuous

² Here it is assumed that the gain is inhomogeneously broadened, which is well fulfilled in quantum well semiconductor lasers, where also spatial hole burning is weakened by the free mobility of charge carriers along the optical propagation direction. This assumption would be much less justified in quantum dot lasers, where gain competition is much reduced and spatial hole burning can become a strong effect.

tuning range than one FSR of the laser cavity, $\Delta\lambda_c$. Extending the cavity length for a narrower laser linewidth would reduce the FSR and thus reduce this limit of continuous tuning.

To prevent such a mode hop and thereby extend the continuous tuning range beyond the limit of one FSR, it is required to tune the transmission of both microring resonators as well, in suitable synchronism. The goal of tuning the microrings is to impose and maintain larger roundtrip losses for all other modes except the for the oscillating mode with order m . The effect of tuning the microring resonators will be described in the next section.

2.4 Microring resonator

The type of hybrid lasers investigated here may contain two microring resonators inside the laser cavity (*e.g.*, as in Fig. 1.1). Here we describe wavelength tuning of a single microring as a prototype example. The goal is to provide expressions for the tuning sensitivity of the resonant microring wavelength and for the tuning sensitivity of the laser cavity wavelength, when tuning the microring. We will find that the effective length contribution of the microring inside the laser cavity plays an important role in these equations.

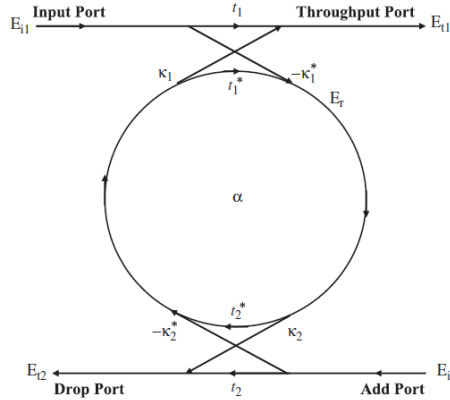


Fig. 2.1: Model of an add-drop ring resonator^[33].

Fig. 2.1 shows a schematic of a microring as used in the loop mirror of the laser cavity. Light is incident at the input port and via a coupler coupled into the ring described in the most general case with complex coupling coefficient κ_1 . The remainder is transmitted to the throughput port with complex transmission t_1 . Light coupled into the ring starts to circulate inside the ring and is coupled out at a second coupler, located at half a roundtrip from the first coupler, with coupling coefficient κ_2 and transmitted with transmission coefficient t_2 . In the remainder we consider the two couplers to be identical, symmetric and loss-free, *i.e.*, $\kappa_1 = \kappa_2 \equiv i\kappa$ and $t_1 = t_2 \equiv t$ with both κ and t real quantities and $\kappa^2 + t^2 = 1$.

For light circulating inside the microring resonator, the roundtrip phase, $\theta_{rt,r}$, and the resonance condition are formally identical to those of the standing wave (linear) laser cavity (Eqs. 2.3 and 2.8), except that the length $L_{rt,r}$ is the geometrical roundtrip length of the resonator. Hence, the resonance condition becomes

$$\theta_{rt,r} = \frac{2\pi L_{rt,r} n_{\text{eff}}(\lambda_r)}{\lambda_r} = m_r 2\pi, \quad (2.12)$$

where λ_r is the wavelength of longitudinal mode m_r inside the microring resonator. In general, $m_r < m_c$ because the roundtrip length of the intra-cavity ring resonator is generally smaller than the roundtrip length of the laser cavity.

As shown in appendix A.1, we obtain for the FSR of a ring resonator

$$\Delta\lambda_r = \frac{\lambda_r^2}{n_g(\lambda_r)L_{rt,r}}. \quad (2.13)$$

Adding a tunable phase shift, ϕ_r , that can be adjusted, *e.g.*, via a heater on top of the ring resonator, the resonance condition becomes

$$\theta_{rt,r} = \frac{2\pi L_{rt,r} n_{\text{eff}}(\lambda_r)}{\lambda_r} + \phi_r = m_r 2\pi. \quad (2.14)$$

The tuning sensitivity of the resonant wavelength of the ring resonator, $\frac{\partial\lambda_r}{\partial\phi_r}$, can now be expressed in a similar way as the tuning sensitivity for the phase section (see appendix A.2),

$$\frac{\partial\lambda_r}{\partial\phi_r} = \frac{\Delta\lambda_r}{2\pi}. \quad (2.15)$$

To find how the resonant laser wavelength, λ_c , changes with the extra phase due to the heater on top of the microring, *i.e.*, the tuning sensitivity $\frac{\partial\lambda_c}{\partial\phi_r}$, we start with the phase shift between the input and drop port of the microring. Light leaving the drop port will have attained an increase in optical phase of θ_d with respect to the light incident on the input port. According to Eq. 2.4, this corresponds to an effective geometric length^[21] $L_{\text{eff},r}(\lambda_c)$ inside the ring given by

$$\theta_d(\lambda_c) = \beta L_{\text{eff},r}(\lambda_c) = \frac{2\pi n_{\text{eff}}(\lambda_c) L_{\text{eff},r}(\lambda_c)}{\lambda_c}, \quad (2.16)$$

where the length of the linear laser cavity is increased by $L_{\text{eff},r}(\lambda_c)/2$. The next step is to find an expression for this effective length of the ring resonator inside the laser cavity. In appendix A.3 a relation for this length is derived (see Eqs. A.16-A.22), giving

$$L_{\text{eff},r}(\lambda_c) \approx L_{rt,r} \frac{\partial\theta_d}{\partial\theta_{rt,r}} \quad (2.17)$$

Equation 2.17 shows that the effective length of the ring resonator is equal to the roundtrip length of the ring resonator times the change in phase of the light at the drop port with respect to a change in phase of the recirculating light inside the ring. The optical phase advance of the light from input port to drop port is given by (see appendix A.3, Eqs. A.23-A.26)

$$\theta_d = \text{Arg} \left(\frac{-\kappa^2}{e^{-\frac{1}{2}j\theta_{rt,r}} - (1-\kappa^2)e^{\frac{1}{2}j\theta_{rt,r}}} \right). \quad (2.18)$$

Equation 2.18 can in principle be used to calculate $\frac{\partial\theta_d}{\partial\theta_{rt,r}}$ and thereby to find the effective length of the ring resonator using Eq. 2.17. However, it is more illustrative to show how the effective length $L_{\text{eff},r}$ changes when the roundtrip phase changes over a range of 2π , *i.e.*, corresponding to one full FSR of the ring resonator. As can be seen in Fig. 2.2, when decreasing κ^2 , the effective length of the ring resonator, and consequently also the length of the laser cavity, becomes largely enhanced at the resonances of the ring resonator, where $\theta_{rt,r} = n2\pi$.

Starting from Eq. 2.18, a more specific relation for $\frac{\partial\theta_d}{\partial\theta_{rt,r}}$ can be derived for the ring resonator near the resonances (see appendix A.3, Eqs. A.26-A.32),

$$\frac{\partial\theta_d}{\partial\theta_{rt,r}} \approx \left(\frac{1}{2} + \frac{1-\kappa^2}{\kappa^2} \right). \quad (2.19)$$

Substituting Eq. 2.19 into Eq. 2.17 results in

$$L_{\text{eff},r} \approx L_{\text{rt},r} \left(\frac{1}{2} + \frac{1-\kappa^2}{\kappa^2} \right). \quad (2.20)$$

Equation 2.20 shows that the effective length of a ring resonator is enhanced by a factor of $\frac{1}{2} + \frac{1-\kappa^2}{\kappa^2}$ on resonance. The geometrical distance between the input and drop port is just half a roundtrip length, which explains the factor $\frac{1}{2}$. Added to this is the increase in effective length, by a factor of $\frac{1-\kappa^2}{\kappa^2}$, caused by light travelling around in the ring resonator many times at resonance, before it is coupled out. Equation 2.20 describes the effective length contribution of the microring inside the laser cavity, restricted by the condition that it is only valid for near resonance operation.

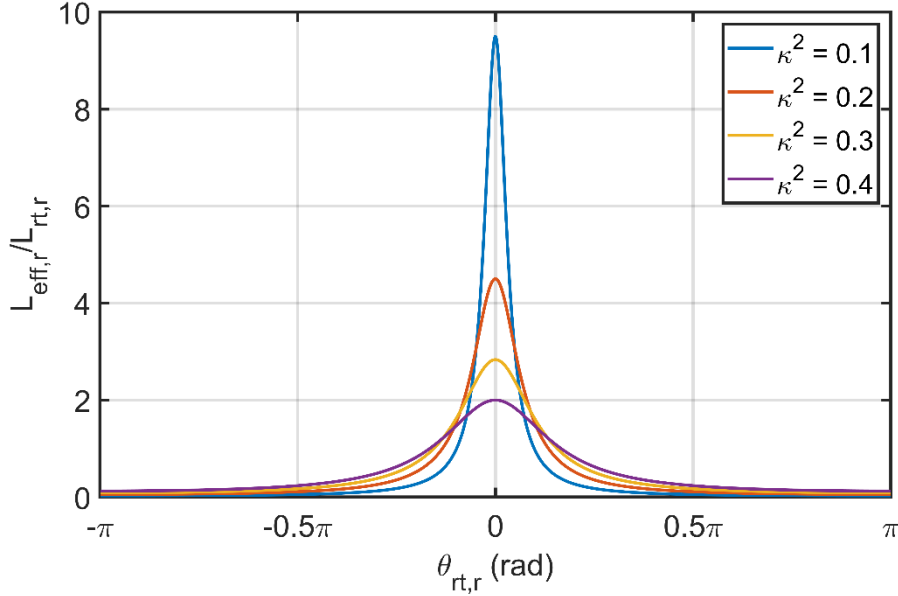


Fig. 2.2: Effective length of a microring resonator inside a laser cavity, $L_{\text{eff},r}$, compared to the roundtrip length of the same microring resonator, $L_{\text{rt},r}$, as function of the roundtrip phase $\theta_{\text{rt},r}$ from $-\pi$ to π , for different values of the coupling coefficient κ^2 between the bus and ring waveguide.

When the ring resonator inside the loop mirror is tuned, not only does the resonant wavelength of the ring resonator change, but also the resonant wavelength of the laser cavity. As with the phase section, we assume that tuning of the ring resonator induces an additional phase ϕ_r on the propagating light inside the ring. Using Eq. 2.17 we obtain

$$\frac{\partial \theta_d}{\partial \phi_r} = \frac{\partial \theta_d}{\partial \theta_{\text{rt},r}} = \frac{L_{\text{eff},r}(\lambda_c)}{L_{\text{rt},r}}, \quad (2.21)$$

as Eq. 2.17 remains valid whether the change in phase of the light is from a change in wavelength or from an added phase due to heater on top of the ring resonator. For the change in resonant wavelength, λ_c of the laser cavity we now can write

$$\frac{\partial \lambda_c}{\partial \phi_r} = \frac{\partial \lambda_c}{\partial \theta_d} \frac{\partial \theta_d}{\partial \phi_r} = \frac{\partial \lambda_c}{\partial \theta_d} \frac{L_{\text{eff},r}(\lambda_c)}{L_{\text{rt},r}}. \quad (2.22)$$

The effect of a phase change at the drop port of the ring resonator, $\Delta \theta_d$, on the cavity wavelength is one half of the effect of the phase change by setting the phase section, $\Delta \phi_{\text{ps}}$, because the phase section is passed twice per laser roundtrip, while the ring resonator is passed once per roundtrip. Using this, we can rewrite Eq. 2.22 as (*cf.* Eq. 2.11)

$$\frac{\partial \lambda_c}{\partial \phi_r} = \frac{\partial \lambda_c}{\partial \phi_{\text{ps}}} \frac{1}{2} \frac{L_{\text{eff},r}(\lambda_c)}{L_{\text{rt},r}} = \frac{\Delta \lambda_c}{2\pi} \frac{L_{\text{eff},r}(\lambda_c)}{L_{\text{rt},r}}. \quad (2.23)$$

Combining Eqs. 2.20 and 2.23 finally gives the tuning sensitivity of how the resonant laser wavelength changes with the extra phase due to the heater on top of a microring,

$$\frac{\partial \lambda_c}{\partial \phi_r} \approx \frac{\Delta \lambda_c}{2\pi} \left(\frac{1}{2} + \frac{1-\kappa^2}{\kappa^2} \right). \quad (2.24)$$

If we compare the shift in resonant wavelength due to tuning the ring resonator (Eq. 2.24) with the shift resulting from tuning the phase section (Eq. 2.11), we observe that tuning of the ring resonator enhances the change in resonant wavelength by a factor of $\frac{1}{2} \left(\frac{1}{2} + \frac{1-\kappa^2}{\kappa^2} \right)$. Therefore, to shift the laser wavelength with the same amount, the ring heater needs to induce a much smaller phase change ϕ_r compared to the phase ϕ_{ps} induced by the phase section heater.

2.5 Vernier filter

For stable single-mode operation of a semiconductor laser with a broad gain bandwidth, for the laser investigated here in the order of 100 nm, a filter FSR is required of at least this value. There are two ways to obtain a large filter FSR. One method is to reduce the roundtrip length of the microring resonator because the FSR is inversely proportional to the roundtrip length (*cf.* Eq. 2.13). However, decreasing the roundtrip length requires a decreasing ring radius, which results in a significant increase in bending loss and this limits the spectral selectivity. Another well-known approach, as used in the laser investigated here, is to use two ring resonators in series with a slightly different FSR. This increases the wavelength spacing between the filter transmission peaks, without reducing the bend radii, based on the Vernier effect. The resulting FSR of the Vernier filter, $\Delta \lambda_V$, is then given by^[34]

$$\Delta \lambda_V \equiv M_{r1} \Delta \lambda_{r1} = M_{r2} \Delta \lambda_{r2} \quad (2.25)$$

where M_{r1} and M_{r2} are integers and need to be coprime for obtaining $\Delta \lambda_V$. Note that these integers should not be confused with the longitudinal mode numbers m_{r1} and m_{r2} of the microring resonators. By rewriting Eq. 2.25 we obtain

$$\Delta \lambda_V = (M_{r2} - M_{r1}) \frac{\Delta \lambda_{r1} \Delta \lambda_{r2}}{\Delta \lambda_{r1} - \Delta \lambda_{r2}}. \quad (2.26)$$

A suitable Vernier filter transmission curve can be found under the condition of $M_{r2} - M_{r1} = 1$ ^[23]. Substituting this condition in Eq. 2.26 gives

$$\Delta \lambda_V = \frac{\Delta \lambda_{r1} \Delta \lambda_{r2}}{|\Delta \lambda_{r1} - \Delta \lambda_{r2}|}, \quad (2.27)$$

showing that the resulting Vernier FSR is largely increased when the difference between the microring FSRs is small. To find the required ratio between the roundtrip lengths of both microring resonators, we substitute Eq. 2.25 in Eq. 2.13 and find that

$$L_{rt,r2} = \frac{M_{r2}}{M_{r1}} L_{rt,r1}, \quad (2.28)$$

under the assumption that both rings are identical except for the ring circumference. Filling in Eq. 2.28 in the resonance condition Eq. 2.12 for both ring resonators gives a similar condition for the longitudinal mode numbers

$$m_{r2} = \frac{M_{r2}}{M_{r1}} m_{r1}. \quad (2.29)$$

Because M_{r1} and M_{r2} are coprime integers, common resonances occur only for longitudinal mode numbers fulfilling the condition, $m_{r1} = m_V M_{r2}$ and $m_{r2} = m_V M_{r1}$ where m_V is an integer, describing the order of the common Vernier transmission. This significantly reduces the available mode numbers. Therefore, the continuous tuning condition, Eq. A.12, remains fulfilled over a larger

tuning range, namely the Vernier FSR. For continuous tuning of the Vernier filter peak, both ring resonances have to be tuned synchronously while maintaining $\delta\lambda_{r1} = \delta\lambda_{r2}$. Using Eqs. 2.15, 2.25 and 2.28 we obtain the tuning ratio for the two rings as

$$\left(\frac{\delta\phi_{r1}}{\delta\phi_{r2}}\right)_V = \frac{\Delta\lambda_{r2}}{\Delta\lambda_{r1}} = \frac{L_{rt,r1}}{L_{rt,r2}} = \frac{M_{r1}}{M_{r2}} \quad (2.30)$$

for continuous tuning of the Vernier filter transmission peak.

2.6 Mode-hop-free tuning

Now that we have provided expressions for tuning of the resonant laser wavelength via the phase section and ring resonators separately, we consider the synchronous tuning of the phase section and both ring resonators. First, we observe for tuning the cavity resonant wavelength by the phase section

$$\delta\lambda_{c,ps} = \frac{\partial\lambda_c}{\partial\phi_{ps}} \delta\phi_{ps} = \frac{\Delta\lambda_c}{\pi} \delta\phi_{ps}, \quad (2.31)$$

and we know from Eq. 2.23 the resonant wavelength shift in each ring resonator. When all three elements are tuned at the same time, we have three contributions to the change in cavity resonant wavelength, $\delta\lambda_c$

$$\delta\lambda_c = \frac{\partial\lambda_c}{\partial\phi_{ps}} \delta\phi_{ps} + \frac{\partial\lambda_c}{\partial\phi_{r1}} \delta\phi_{r1} + \frac{\partial\lambda_c}{\partial\phi_{r2}} \delta\phi_{r2}, \quad (2.32)$$

due to the phase section and the ring resonators 1 and 2. For mode-hop-free tuning we require that

$$\delta\lambda_c = \delta\lambda_{r1} = \delta\lambda_{r2}, \quad (2.33)$$

Combining Eqs. 2.15 and 2.33, we obtain for each ring resonator

$$\delta\phi_r = \frac{2\pi}{\Delta\lambda_r} \delta\lambda_c. \quad (2.34)$$

Substituting Eq. 2.34 into Eq. 2.32 and using Eqs. 2.11, 2.13 and 2.23, we obtain

$$\delta\lambda_c = \frac{\Delta\lambda_c}{\pi} \delta\phi_{ps} + \frac{\Delta\lambda_c n_g(\lambda_c)}{\lambda_c^2} \left(L_{\text{eff},r1}(\lambda_c) + L_{\text{eff},r2}(\lambda_c) \right) \delta\lambda_c \quad (2.35)$$

where we have used that $\lambda_{r1} = \lambda_{r2} = \lambda_c$ for the case of mode-hop-free tuning. Solving Eq. 2.35 for $\delta\lambda_c$ gives

$$\delta\lambda_c = \left[\frac{\pi}{\Delta\lambda_c} + \frac{\pi n_g(\lambda_c)}{\lambda_c^2} \left(L_{\text{eff},r1}(\lambda_c) + L_{\text{eff},r2}(\lambda_c) \right) \right]^{-1} \delta\phi_{ps}. \quad (2.36)$$

Finally, using Eq. 2.9, we obtain

$$\delta\lambda_c = \frac{\lambda_c^2}{\pi n_g(\lambda_c)} \frac{1}{2L'_{\text{eff},c}(\lambda_c) - (L_{\text{eff},r1}(\lambda_c) + L_{\text{eff},r2}(\lambda_c))} \delta\phi_{ps}, \quad (2.37)$$

and the tuning sensitivity for mode-hop-free tuning is given by

$$\left(\frac{\partial\lambda_c}{\partial\phi_{ps}}\right)_{\text{MHF}} = \frac{\lambda_c^2}{\pi n_g(\lambda_c)} \frac{1}{2L'_{\text{eff},c}(\lambda_c) - (L_{\text{eff},r1}(\lambda_c) + L_{\text{eff},r2}(\lambda_c))}, \quad (2.38)$$

or, alternatively,

$$\left(\frac{\partial\lambda_c}{\partial\phi_{ps}}\right)_{\text{MHF}} = \frac{\Delta\lambda_c}{\pi} \frac{L'_{\text{eff},c}(\lambda_c)}{L'_{\text{eff},c}(\lambda_c) - \frac{1}{2}(L_{\text{eff},r1}(\lambda_c) + L_{\text{eff},r2}(\lambda_c))}. \quad (2.39)$$

For a discussion of this result we recall that when tuning the resonant laser wavelength using the phase section alone, the maximum mode-hop-free tuning was the free spectral range, $\Delta\lambda_c$ of the laser cavity. Equations 2.38 and 2.39 show that now the mode-hop-free tuning range is different. By including the two rings in the laser cavity, the mode-hop-free tuning range is increased by a factor equal to the ratio of the roundtrip cavity length, $L'_{\text{eff},c}$, to the roundtrip cavity length minus half the sum of the effective lengths of the microring resonators. Therefore, to maximize the mode-hop-free tuning range, the effective length of the microring resonators should be the dominant contribution to the roundtrip length of the laser cavity, *i.e.*, the gain and bus waveguides should be as short as possible.

The denominator in Eqs. 2.38 and 2.39 is equal to the weighted sum of the length of the SOA, the phase section and the bus waveguide. This means that both equations describe that the tuning sensitivity of the hybrid laser is equal to the same laser without the ring resonators adding optical length, *i.e.*, a laser with a much higher tuning sensitivity equal to that of a much shorter laser. Consequently, the hybrid laser provides the tuning range, *i.e.*, one FSR for a 2π phase shift of the propagating light, of a short laser while the intrinsic linewidth is that of a laser with a long cavity. The reason for this effect to occur is the synchronous tuning of the phase section and the rings, which increases the total phase shift experienced by the light for one roundtrip, compared to tuning of the phase section alone. The mode-hop-free tuning further assures that the total phase shift is not limited to 2π any more, and continuous tuning over a larger range is now possible.

For finding the synchronous tuning ratio of the ring resonators versus the phase section, that gives mode-hop-free tuning, we combine Eqs. 2.15 and 2.33 and find for the ring resonators that

$$\left(\frac{\partial\lambda_c}{\partial\phi_r}\right)_{\text{MHF}} = \frac{\Delta\lambda_r}{2\pi}. \quad (2.40)$$

which is similar to the tuning of the resonant wavelength of the ring resonator. Merging Eqs. 2.7, 2.13, 2.39 and 2.40 gives the tuning ratio of the first ring resonator versus the phase section

$$\left(\frac{\partial\phi_{r1}}{\partial\phi_{\text{ps}}}\right)_{\text{MHF}} = \frac{L_{\text{rt},r1}}{L'_{\text{eff},c}(\lambda_c) - \frac{1}{2}(L_{\text{eff},r1}(\lambda_c) + L_{\text{eff},r2}(\lambda_c))} = \frac{L_{\text{rt},r1}}{\frac{n_{g,\text{SOA}}}{n_{g,\text{Si}_3\text{N}_4}}L_{\text{SOA}} + L_{\text{bus}}}. \quad (2.41)$$

A similar expression can be derived for the synchronous tuning of the second ring versus the phase section. In common designs for a laser feedback circuit based on microring resonators, including the laser described here, evaluating Eq. 2.41 will result in $\left(\frac{\partial\phi_{r1}}{\partial\phi_{\text{ps}}}\right)_{\text{MHF}} \ll 1$. Hence, the amount of phase shift applied by the phase section has to be much larger than the phase shift applied by the ring resonator. To optimize a feedback circuit for the technical realization of mode-hop-free tuning, it would be beneficial if these phase shifts are of the same order, so that evaluating Eq. 2.41 results in ≈ 1 . This could be realized by designing the feedback circuit according to $L_{\text{rt},r} \approx \frac{n_{g,\text{SOA}}}{n_{g,\text{Si}_3\text{N}_4}}L_{\text{SOA}} + L_{\text{bus}}$, by choosing a sufficiently large $L_{\text{rt},r}$ and by minimizing L_{bus} . However, the drawback of increasing $L_{\text{rt},r}$ is that it also reduces the microring FSR (*cf.* Eq. 2.13) and therefore complicates a proper design of the Vernier filter.

To find the maximum mode-hop-free tuning range, we consider the three conditions that limit this range. First, in a feedback circuit where the maximum phase shift is the same for every tuning element, and where $\left(\frac{\partial\phi_{r1}}{\partial\phi_{\text{ps}}}\right)_{\text{MHF}} \ll 1$, the mode-hop-free tuning range is technically limited by the phase section. By recalling that the change in laser wavelength is given by $\Delta\lambda = \frac{\partial\lambda}{\partial\phi}\Delta\phi$, we obtain the

maximum mode-hop-free tuning range, $\Delta\lambda_{\text{MHF,max}}$, as (*cf.* Eq. 2.39)

$$\Delta\lambda_{\text{MHF,max}} \leq \frac{\Delta\lambda_c}{\pi} \frac{L'_{\text{eff},c}(\lambda_c)}{L'_{\text{eff},c}(\lambda_c) - \frac{1}{2}(L_{\text{eff},r1}(\lambda_c) + L_{\text{eff},r2}(\lambda_c))} \Delta\phi_{\text{ps,max}}. \quad (2.42)$$

Second, in any feedback circuit, the maximum mode-hop-free tuning range is technically limited by the continuous tuning range of the microring resonances. So, the maximum range is limited by the maximum phase shift that can be applied on either one of the ring resonators via (*cf.* Eq. 2.15)

$$\Delta\lambda_{\text{MHF,max}} \leq \frac{\Delta\lambda_r}{2\pi} \Delta\phi_{r,\text{max}}. \quad (2.43)$$

Third, and finally, synchronous tuning of the Vernier filter is physically limited to the Vernier FSR, as described in section 2.5. As the mode-hop-free tuning method depends on the continuous tuning of the Vernier filter, the tuning range is ultimately limited by the Vernier FSR, *i.e.*,

$$\Delta\lambda_{\text{MHF,max}} \leq \Delta\lambda_V. \quad (2.44)$$

For any design of a laser feedback circuit based on microring resonators, the smallest value resulting from evaluation of either Eqs. 2.42, 2.43 or 2.44 restricts the mode-hop-free tuning range.

3 Laser device and set-up

3.1 Hybrid integrated laser

The hybrid laser was already coarsely described in the introduction. Here we provide a more complete description of the laser and its driving electronics. The schematic representation of the laser circuit shown in Fig. 1.1 comprises an InP-based RSOA gain chip and the Si₃N₄-based feedback chip with a mirror and Vernier filter based on two microring resonators. Using the relations given in chapter 2, we discuss here the design choices for the integrated hybrid diode laser.

Two different material platforms are used for the fabrication of the photonic chips that are combined via hybrid integration to form the laser. There are several major material platforms in integrated photonics, such as Silicon-on-Insulator (SOI), the III-IV semiconductors, e.g. InP, and Silicon Nitride (Si₃N₄). Each platform has its specific advantages, making it suitable for certain functionalities or applications. For example, SOI is compatible with existing processing facilities for electronics and its high index contrast allows for integration of many components on small chips^[35]. The III-IV semiconductor platform excels in the integration of light sources, high-speed modulators and detectors on a chip^[36]. For Si₃N₄, the main advantage is that it offers a good balance between the moderately tight confinement of the waveguide modes in combination with very low propagation losses, making this platform very suitable for high-quality microring resonators^[37]. The combination of several requirements can be a major challenge for any single material platform. For example, the combination of light sources with low-loss waveguides is not easy to meet, because no single platform excels in both. For building a laser with low intrinsic linewidth, both properties are required. Light has to be amplified and a long, low-loss laser cavity is required for achieving a low linewidth. To fulfill both requirements in the same device, the laser described here is based on hybrid integration, benefitting from the best of two specific platforms: the light generation functionality of InP and the low propagation losses from Si₃N₄.

Table 3.1. Design parameters of the hybrid laser, specified around the operating wavelength of 1550 nm.

Symbol	Value	Description
λ_c	1550 nm	Operating wavelength (nominal value)
$n_{\text{eff,SOA}}$	3.155	Effective index of the SOA
$n_{\text{g,SOA}}$	3.6	Group index of the SOA
$n_{\text{eff,Si}_3\text{N}_4}$	1.535	Effective index of Si ₃ N ₄ feedback circuit waveguides
$n_{\text{g,Si}_3\text{N}_4}$	1.715	Group index of Si ₃ N ₄ feedback circuit waveguides
L_{SOA}	0.7 mm	Single-pass geometrical length of the SOA
L_{bus}	6.7 mm	Single-pass geometrical bus waveguide length
$L_{\text{rt,r1}}$	885.1 μm	Roundtrip length of MRR 1
$L_{\text{rt,r2}}$	857.4 μm	Roundtrip length of MRR 2
κ^2	0.10	Power coupling coefficient between bus and MRR

The SOA chip, fabricated by the Fraunhofer Heinrich Hertz Institute (HHI)^[38], contains a multi-quantum well active waveguide, based on InP, functioning as an optical amplifier with a gain bandwidth of > 100 nm around 1550 nm. One facet of this chip has a high-reflection (HR) coating of $\sim 90\%$ reflectivity against air, which forms one of the feedback mirrors of the laser cavity. At the other facet, light is coupled to the Si₃N₄ chip, which forms the other feedback mirror. To reduce undesired reflections from the interface between the two chips, two measures are taken. One is an anti-reflection (AR) coating applied at the interface facet and the other is a tilt of 9° of the waveguide with the facet normal. Other design parameters for the InP chip can be found in Table 3.1.

The Si₃N₄ chip forms the remaining part of the hybrid laser cavity. This chip is based on the TriPleX symmetric double-stripe (SDS) waveguide^[39]. This waveguide geometry consists of two 1.2 μm wide and 170 nm thick Si₃N₄ stripes, with a 500 nm thick layer of SiO₂ in between. The waveguide is single-mode, optimized for small bend radii, down to 100 μm, and offers very low propagation losses (<0.1 dB/cm). The effective index and group index at the nominal wavelength of 1550 nm are also specified in Table 3.1, together with other parameters for the Si₃N₄ chip. One of the main advantages of the Si₃N₄ platform is that the waveguides can be tapered two-dimensionally for optimal matching of the optical mode to the mode of another chip or an optical fiber. This involves vertical tapering, by reducing the thickness of both Si₃N₄ layers to 35 nm. At the facet for coupling with the RSOA, the waveguide is tapered two-dimensionally and angled down with 19.85° with respect to the facet normal to match the InP waveguide optical mode and angle at the interface. This mode and angle matching allows efficient coupling and reduces spurious reflections to a minimum.

Based on these TriPleX SDS waveguides, a set of lithographic masks of the feedback circuit with dedicated heaters was designed, as shown in Fig. 3.1 (a), which implements the schematic circuit shown in Fig. 1.1. The waveguide circuit contains two racetrack-shaped microring resonators, which serve as a frequency selective mirror. The designed roundtrip lengths, as presented in Table 3.1 are nearly the smallest lengths possible based on the chosen implementation of racetrack resonators with adiabatic bends and the requirement of bend radii of at least 100 μm. This choice of slightly different roundtrip lengths results in FSRs of 1.58 nm and 1.63 nm, respectively for the two microrings. By utilizing the Vernier effect with two cascaded resonators and by using the ratio $\frac{M_{r2}}{M_{r1}} = \frac{32}{31}$, the total FSR, $\Delta\lambda_V$, is 50.5 nm around the nominal wavelength. Even though this FSR is smaller than the gain bandwidth of the InP chip, this filter severely restricts the possible modes at which the laser can operate. Assisted by additional filtering, as described in section 4.1, single-mode operation is provided across the full gain bandwidth.

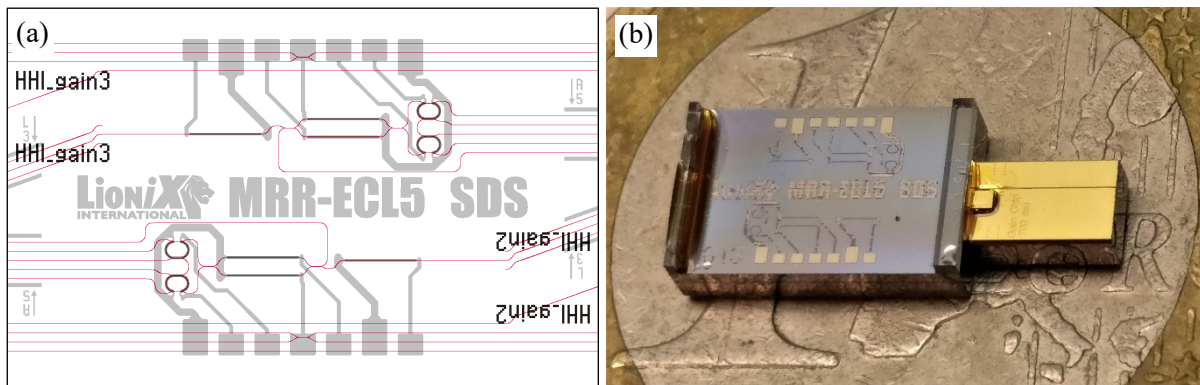


Fig. 3.1. (a) Mask design of the Si₃N₄ feedback chip, showing two identical feedback circuits with different interfaces for two different gain chips. The lower half of this design is used for the laser investigated here. (b) Hybrid assembly of the laser photonic chip, on top of a one Euro coin. The left part is the Si₃N₄ feedback chip, while the right part is the SOA on top of a submount.

To extract an adjustable fraction of the light from the cavity, a tunable Mach-Zehnder interferometer is placed inside the cavity, which functions as a tunable coupler with coupling ratios between 0 and 100%. The tunable coupler together with the Vernier filter can be considered as the second feedback mirror of the laser cavity, with a tunable and wavelength-dependent reflectivity. Via the tunable coupler, part of the light circulating inside the cavity can be directed toward the output facet. At this output facet, the waveguide is tapered two-dimensionally for optimal coupling with a single mode fiber, which forms the output of the laser. Tuning any element, *e.g.*, the amplifier, ring resonators and tunable coupler, also changes the phase of the light circulating inside the cavity. To compensate for these phase changes and to control the cavity roundtrip phase, a so-called tunable phase section is added to the circuit as well.

For tuning all elements in the feedback circuit as required, five resistive heaters are placed on top of the waveguides. The effect of the heaters is to add a tunable optical phase, as we describe in section 2.2. Heaters are placed on both ring resonators, the tunable coupler (two heaters, one on each MZI branch) and the phase section. Each heater is connected with a lead to corresponding bond pads for a ground and signal voltage. The heaters and leads are based on a platinum and gold layer stack. The platinum heaters can, according to the manufacturer, be driven with electrical currents up to approximately 85 mA before breaking down. In order not to damage the laser, we limit the current here to a value of 70 mA. As described in section 4.2, this limits the dissipated power in the heaters on the microrings to approximately 600 mW, enabling nearly 2π phase tuning, and approximately 700 mW on the other heaters, enabling more than 2π phase tuning.

In order to assemble the hybrid laser, the following steps are carried out. Glass rails are glued on top of the Si_3N_4 chip to facilitate polishing. Both facets are polished, to decrease the facet roughness after dicing. The InP chip, placed on a submount, which serves as a heatsink, is then aligned and glued to the glass chip. The resulting hybrid assembly is shown in Fig. 3.1 (b) on top of a one Euro coin, to indicate the size of the hybrid integrated laser.

3.2 Butterfly package and PCB

The full hybrid laser is assembled in a 14-pin butterfly package as shown in Fig. 3.2 (a). This butterfly package contains a Peltier element and thermistor for temperature control and stabilization of the laser chip. The bond pads on the chip are wire bonded to the butterfly pins such that these pins can be used for electrical access to the SOA and heaters. A single-mode polarization maintaining fiber is attached to the output waveguide of the laser chip. This fiber is terminated with an FC/APC connector, which has an angled facet to prevent undesired reflections back into the laser.

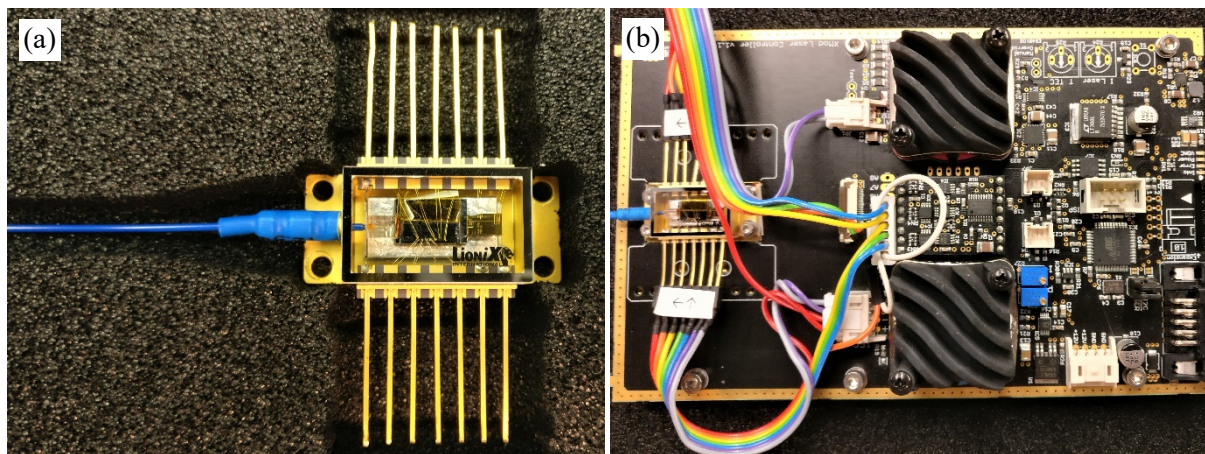


Fig. 3.2. (a) Photo of the hybrid laser and output fiber assembled in a 14 pin butterfly package with Peltier element and thermistor for temperature control. (b) Photo of the butterfly package placed on top of a printed circuit board for controlling the laser, with a current source, Peltier controller and various DACs, all controlled by a microcontroller and connected via a USB-interface to a computer.

For controlling the laser, LioniX has developed a printed circuit board (PCB) as shown in Fig. 3.2 (b). This PCB contains a temperature controller for controlling the Peltier element with temperature feedback from a thermistor. It also contains a current source to provide the SOA with a constant current. To control the voltages to the various heaters, an 8-channel, 16-bits DAC is placed on the board. A microcontroller is used for operating the board through messages via an USB-interface connected to a computer. The butterfly package is mounted via a thermal heatsink, on top of this PCB and electrically connected with the corresponding voltage, current and Peltier drivers. The PCB serves as a control station to operate the laser via a computer, enabling accurate and reproducible control of laser operation.

3.3 Experimental set-up

The experimental setup used to characterize the laser in terms of output power, wavelength and linewidth, is schematically shown in Fig. 3.3. The output fiber of the laser is connected with a fiber isolator (Thorlabs IO-G-1550-APC) to prevent undesired external reflections back into the laser. The laser light is then equally divided by a 50:50 fiber optical coupler (Thorlabs TW1550R5A2). One of the outputs of the splitter is connected with an integrating sphere photodiode (Thorlabs S144C). All measured values on the photodiode are compensated for the measured transmission loss through the isolator and the splitter of 3.87 dB. The other output is again split in two by a 95:5 fiber optic coupler (AOFR WBY05131510aSR). For measuring the linewidth, the largest part, 95%, is sent to a delayed self-heterodyne (DSH) measurement setup. This setup consists of an unbalanced Mach-Zehnder interferometer, where one arm contains a 20 km long fiber delay line, and the other arm contains an acoustic-optical modulator to induce a frequency shift of 80 MHz, as described in more detail by Fan *et al.*^[24]. The linewidth can be retrieved from the beat signal, detected by a fast photodiode (DSC-R401HG, 20 GHz) connected to a Radio-Frequency Spectrum Analyzer (RFSA, Agilent E4405B). The remainder of the light, 5% from the fiber optic coupler, is sent to an optical spectrum analyzer (OSA). Two different OSAs are used, depending on the required resolution and wavelength range for the measurement. One OSA (ANDO AQ6317) is based on a rotating grating in combination with a slit and has a specified resolution of 15 pm. The other OSA (Finisar WaveAnalyzer 1500S) is based on coherent detection with a scanning laser and has a much smaller resolution bandwidth of 1.4 pm and a sampling resolution of 0.16 pm. To improve the signal to noise ratio in the measured spectra, spectral averaging on this device was set to 16 times.

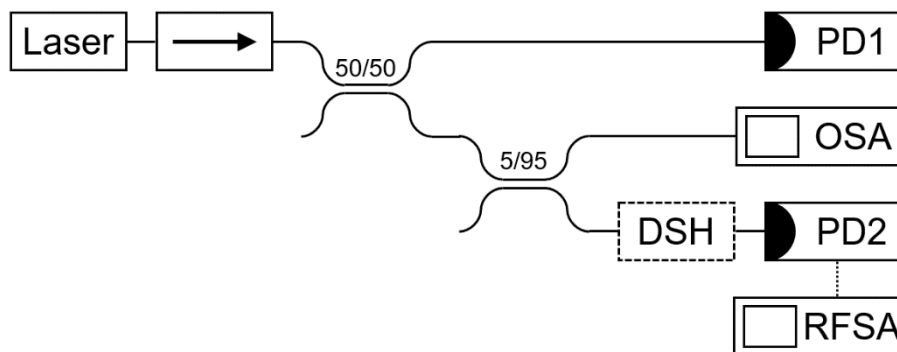


Fig. 3.3. Schematic view of the experimental set-up for characterizing the laser, showing the laser, an isolator (\rightarrow) and a 50/50 fiber optic coupler. One output of the coupler is connected with a photodiode (PD1), while the other output is further divided by a 5/95 fiber optic coupler, where the 5% output is connected to an optical spectrum analyzer (OSA). The 95% output is fed into the delayed self-heterodyne (DSH) linewidth measurement setup, which uses a fast photodiode (PD2) connected to radio-frequency spectrum analyzer (RFSA) for measuring the beat frequency.

For simultaneous operation of all equipment (except the Finisar OSA), we developed a LabVIEW-based program with an interface as shown in Fig. 3.4. This program allows to control the different instruments and retrieve measurement data via either RS232, GPIB and USB interfaces. The laser can be controlled via sliders, each acting at one laser control. In addition to power sensor, OSA and RSA measurements, 1D parameter sweeps can be performed, where one laser setting is varied and simultaneously the output power, wavelength and linewidth are measured at each setting. The measured data can be processed and graphically displayed with the program. For example, the data obtained from the RFSA connected to the self-heterodyne detection setup is automatically processed with a Voigt fit, revealing the Lorentzian and Gaussian linewidth components associated with the spectral output of the laser.

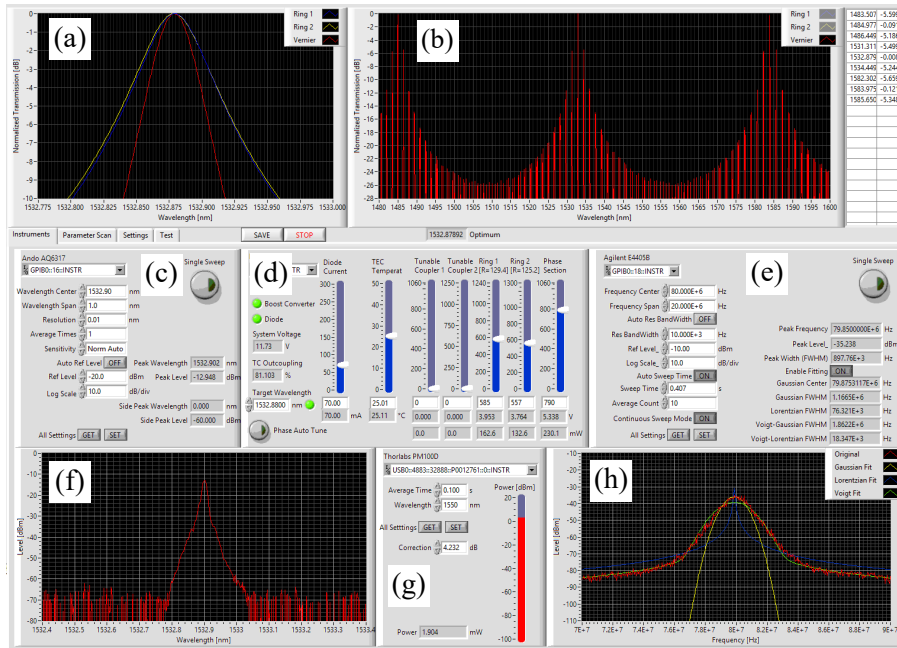


Fig. 3.4. LabVIEW interface for simultaneous operation of the laser with the measurement equipment with (a) a close-up of the modelled Vernier transmission, (b) the modelled Vernier transmission over the full gain bandwidth, (c) control panel of the OSA, (d) control panel of the laser, (e) control panel of the RFSAs for the linewidth measurement with the fitting results, (f) measured graph retrieved from the OSA, (g) control panel of the optical power sensor and (h) measured graph retrieved from the RFSAs with the applied linewidth fits.

To assist tuning of the laser, a physical model of both MRRs in Vernier configuration was added to the LabVIEW program that predicts the laser wavelength as function of tuning these MRRs, as described in more detail in section 4.2.3. This allows comparison of the predicted wavelength with the measurement data obtained from the OSA, and it allows entering a desired laser wavelength to set the MRRs to the required value.

To simplify the setting of the laser, a so-called auto-phase tune function was added. This function sweeps the heater power applied to the phase section and simultaneously measures the output power of the laser. Afterwards, the phase section is set to the heater value, where the output power is maximum, causing the cavity mode to overlap with the common resonance of both microring resonators. The auto-phase tuning can also be used during parameter sweeps, such that the phase section is optimized for each step of the sweep, to compensate an unwanted phase shift of the cavity mode caused by the swept parameter.

Having installed the described hardware and software, the control of the hybrid laser is much improved compared to earlier versions of these lasers. First, the hybrid assembly of the laser in a butterfly package with a Peltier element allows for precise thermal stabilization and obtaining reproducible results. Second, the placement of the butterfly package on a computer controlled PCB allows for systematic control of all laser settings. And third, the LabVIEW interface simplifies retrieving measurement data and allows for fast parameter sweeps. These improvements enable an accurate, reproducible and systematic characterization of the laser, as described in the next chapter.

4 Experimental results

4.1 Laser characteristics

The output characteristics of the laser depend on the interplay between various laser settings. For example, the output power depends on the Peltier temperature, the gain current, the wavelength position of the Vernier transmission peak, the outcoupling set by the tunable coupler, and the setting of the phase section. Changing these settings will affect the wavelength and linewidth of the laser as well. To systematically characterize the properties of the laser, we start presenting the dependence of the output power, threshold current, spectral coverage, side mode suppression ratio and linewidth versus various laser settings.

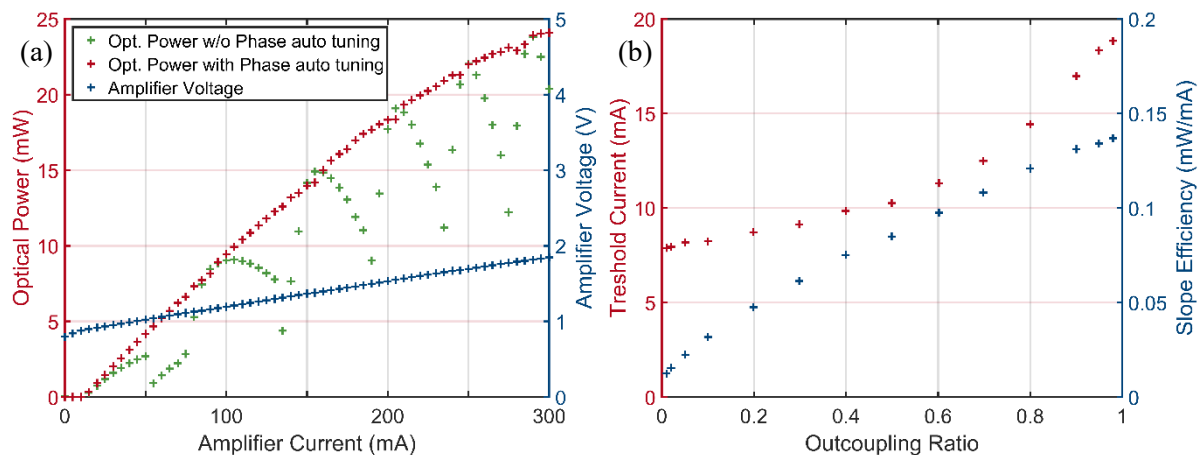


Fig. 4.1. (a) Measured fiber-coupled output power of the laser as function of the amplifier current without tuning the phase section (green data points) and with tuning of phase section (red data points) for each setting of the amplifier current. The corresponding amplifier voltage is shown as blue data points. Power fluctuations due to mode hops are visible when the phase section is not tuned (green data points) and are absent when the phase section is tuned (red data points). For these measurements, the TEC temperature was set to 20° C, the Vernier filter wavelength was set to 1576 nm and the outcoupling to 80%. (b) Threshold current (red) and slope efficiency (blue) measured as function of the outcoupling ratio of the tunable coupler. The amplifier current was swept between 0 and 40 mA to determine both parameters. For this measurement series, the Vernier filter wavelength set to 1557.7 nm and auto tuning of the phase section was applied before every single measurement.

In Fig. 4.1 (a) the fiber-coupled output power of the laser is shown as function of the amplifier current. A coarse scan of different laser settings was first performed to search for the maximum output power. The maximum output power is available at the lowest temperature, 20° C, of the operating temperature range between 20° C and 50° C, as specified by the manufacturer. For all subsequent measurements, the temperature was set to 25° C to guarantee operation above ambient temperature to prevent undesired condensation of ambient air humidity. This setting reduces the maximum output power by only a few percent. Due to the variation of the gain and loss with wavelength, the maximum power also depends on the wavelength setting of the Vernier filter. An initial scan of this filter indicated that the maximum output power can be found around 1575 nm, which likely corresponds to the peak of the net gain curve. Consequently, the Vernier filter was set at approximately this wavelength for determining the maximum output power. Fig. 4.1 (a) shows that only increasing the amplifier current does not always increase the output power when auto-phase tuning is off. Increasing the amplifier current leads to a variety of effects in the gain section^[15]. Amongst these are, a shift in the peak of the gain, a higher free-carrier density, and an increase in temperature due to non-radiative charge carrier recombination. The net results of these effects for our laser is an increase in effective refractive index of the gain section. The increased index effectively adds an extra phase to the propagating light, which changes the alignment of the cavity mode with respect to the Vernier filter peak, which changes the output power. This effect is clearly visible for the green data points of Fig.

4.1 (a) where the phase section was not automatically tuned for maximum output power. If the tuning of the phase section is automatically optimized for maximum output power before every measurement, the phase shift in the gain material becomes counteracted, resulting in a much smoother function of output power versus current, as can be seen as the red data points in Fig. 4.1 (a). We measured a maximum fiber-coupled optical power of 24 mW, which is more than previous reported values of 1.7 mW^[24] and 10 mW^[25] for similar lasers using a two-ring Vernier filter, and it is more than the maximum of 13 mW reported for a laser containing three rings^[26]. An even higher output power will likely be attainable above the maximum safe driving current of 300 mA, as specified by the manufacturer.

The threshold current and slope efficiency of the laser depend strongly on the outcoupling ratio. Fig. 4.1 (b) shows this dependency with a measurement of the threshold current and slope efficiency as a function of the outcoupling ratio of the tunable coupler. The outcoupling ratios used in the experiment were derived from a simplified model for the tunable coupler. The coupler is modelled as a balanced and wavelength-independent Mach-Zehnder interferometer whose outcoupling ratio, η_{tc} , is related to the applied voltage V_{tc} via $\eta_{tc} = \sin(aV_{tc}^2 + b)^2$, where a and b were experimentally determined by sweeping the tunable coupler voltage and measuring the output power of the laser. As can be seen here, increasing the outcoupling ratio increases both the threshold current and the slope efficiency of the laser. We note that the laser can easily become multimode at low outcoupling ratios. A good operating point for single mode behavior with high output power was found for an outcoupling ratio of approximately 80%.

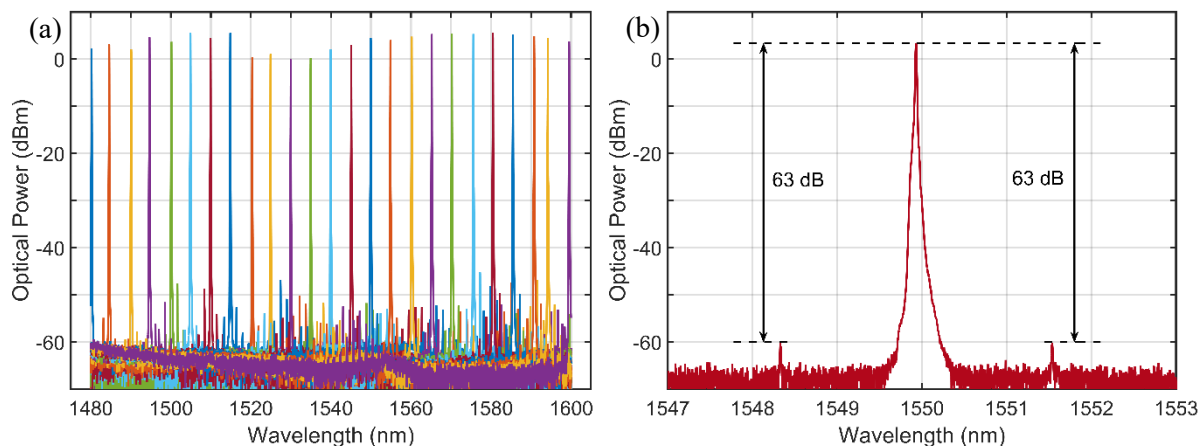


Fig. 4.2. (a) Full tuning range illustrated by superimposed laser spectra showing the optical power in a 0.1 nm resolution bandwidth as measured with the OSA for an amplifier current of 300 mA and an outcoupling of $\sim 80\%$. The Vernier filter is adjusted to obtain lasing at wavelength increments of ~ 5 nm over a range of ~ 120 nm. The phase section was adjusted before each measurement to obtain maximum output power. (b) Measured laser power in a 0.01 nm resolution bandwidth as measured with the OSA, showing a high SMSR of 63 dB. The amplifier current is set to 300 mA, the tunable coupler to $\sim 80\%$ outcoupling, the Vernier filter to 1550 nm and auto-phase tuning is applied. The spectrum is an average of 10 independent measurements to reduce the background noise level and increase the visibility of the side modes.

To demonstrate the broad gain bandwidth and corresponding tuning range of the laser, Fig. 4.2 (a) shows several superimposed laser spectra where the Vernier filter was tuned in steps of approximately 5 nm. The amplifier current was set to its maximum, to obtain the broadest possible tuning range. We note that the Vernier FSR of 50 nm limits normal laser operation to the range between 1530-1580 nm. Although the tunable coupler is designed to be a wavelength-independent balanced Mach-Zehnder interferometer, if no additional phase shift is applied, the fabrication process introduced an optical path length difference between the two arms. Consequently, the coupler becomes wavelength dependent. Fortunately, we can use this dependence to enforce a lasing wavelength outside the normal operating range. This is realized by choosing a setting for the coupler that retains an outcoupling of approximately 80% for the wavelengths of interest but increases outcoupling, and thus the roundtrip

loss, for the wavelengths in the normal operation range of 1530-1580 nm. In this way we were able to extend the total tuning range to 120 nm, which exceeds the Vernier filter FSR by a factor of more than 2. This range is also much broader than the previously reported values of 43.2 nm^[24], 50 nm^[25] and 81 nm^[26].

In order to investigate the single-mode behavior of the laser, we characterized the ratio between the main laser mode and other unwanted modes, also called the side mode suppression ratio (SMSR). The highest SMSR was obtained at a wavelength of 1550 nm and at the maximum gain current of 300 mA. The corresponding spectrum is shown in Fig. 4.2 (b). On both sides of the main laser peak, side modes are visible at a level of 63 dB below the main peak. These side peaks are separated by 1.61 nm in wavelength from the main peak, which matches the average FSR of both ring resonators at 1550 nm. We note that the height of these two side peaks is equal when the filter peaks of both ring resonators and the cavity mode overlap well. This was achieved by iterative tuning of one microring resonator and the phase section, until the output power of the laser was as high as possible. We expected to find the highest SMSR around the peak of the gain curve, around 1575 nm. With the Vernier filter tuned to that wavelength, other laser modes build up around 1525 nm, at one Vernier FSR from the main laser mode, which results in a lower SMSR. When the laser is tuned to 1550 nm, side modes at ~50 nm distance are not detectable with the OSA anymore, possibly because these side modes are suppressed by lower gain or higher losses. The high SMSR of 63 dB that we found indicates proper single-mode lasing. This value has improved compared to previously reported values of 35 dB^[24], 50 dB^[25] and 61 dB^[40] for similar lasers. We believe that our value is higher because of the improved control of the fully packaged laser, which allows to systematically optimize all laser settings.

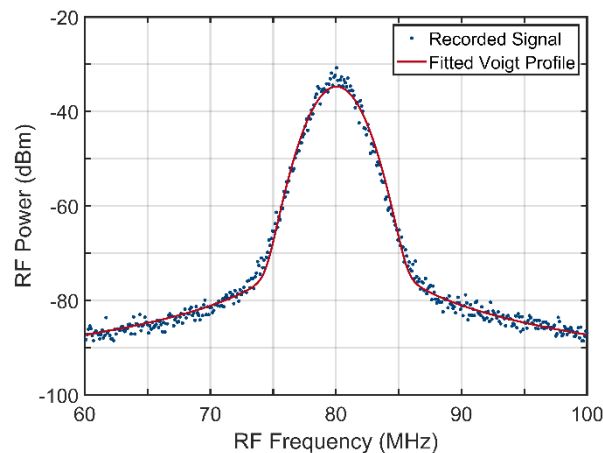


Fig. 4.3. Recorded self-heterodyne beat signal (blue) on the RFSA connected to the laser via the self-heterodyne linewidth measurement setup. The amplifier current is 150 mA, the outcoupling set by the tunable coupler is ~80%, and the Vernier filter is set to 1534.1 nm. The laser phase section is optimized for the smallest linewidth with a slight detuning compared to the setting for maximum output power. The RFSA resolution bandwidth is 10 kHz and averaging is set to 20. Fitting a Voigt profile (red) to the recorded signal reveals a Lorentzian linewidth component of 8 kHz and a Gaussian linewidth component of 1.5 MHz.

A notable feature of this type of hybrid laser is the ultra-narrow intrinsic linewidth, as previously demonstrated. A hybrid laser with a feedback circuit based on three microring resonators provides a record-low intrinsic linewidth of 290 Hz^[26]. To investigate the intrinsic linewidth of this laser, we use the delayed self-heterodyne measurement setup described in section 3.3. The beat between the delayed original laser output and the frequency shifted laser output is measured by a high-speed photodetector connected to a radio-frequency spectrum analyzer (RFSA). In Fig. 4.3, the measured beat signal is shown, from which two linewidth components of the laser can be retrieved. The measured line shape of the RF beat signal can be well approximated with a so-called Voigt profile, which is a convolution of a Gaussian and Lorentzian profile. $1/f$ -noise, often introduced by technical noise, contributes to the Gaussian part of the Voigt profile, while spectrally infinite quantum noise,

e.g., through spontaneous emission, contributes to the Lorentzian part of the profile. The width of this last part is also called the intrinsic linewidth of the laser. In order to find the lowest intrinsic linewidth for this laser, we measured the linewidth at different wavelength settings for the Vernier filter and found that the linewidth is lowest around 1534 nm, where the laser could be operated without applying a voltage to any of the heaters. The latter criterion was applied to reduce also technical noise. When scanning the linewidth as function of the amplifier current, we found that the intrinsic linewidth decreases until a current of about 150 mA, but then remains constant for larger currents. The line shape measurement as presented here is measured around 1534 nm and at a current of 150 mA. By applying a Voigt profile fit to this measurement, we found a Gaussian linewidth component of 1.5 MHz and a Lorentzian component of 8 kHz. The intrinsic (Lorentzian) linewidth of 8 kHz is much smaller than the previously reported values of 25 kHz^[23], 24 kHz^[41], 90 kHz^[24] and 35 kHz^[25] for similar hybrid devices utilizing a two-rings Vernier filter.

Based on this characterization, we conclude that the laser is better in terms of output power, tuning range, SMSR and linewidth compared to previous versions of a hybrid laser with a feedback circuit utilizing two ring resonators. We believe that this improvement is due to the ongoing development and optimization of the hybrid laser technology. For example, the thermal management of the gain chip and the hybrid assembly is improved, which allows higher pump currents. Also, the propagation losses of the feedback chip are reduced, in several ways. The spot size converters are designed to adiabatically change the thickness of the guiding layers, which minimizes the excess loss to below 0.05 dB per spot size converter^{[39], [42]}. The Y-junctions from previous laser designs are replaced with directional couplers or tunable couplers in the current design, which removes the excess loss of the Y-junction due to the gap between the two branches^[39]. The ring resonators are now implemented as racetrack resonators having adiabatic bends. This allows for better control of the coupling coefficient between the bus and ring waveguides and it reduces the mode transition loss between straight and bent waveguides^[39]. The processing of the current feedback chip is based on stepper lithography instead of contact lithography, which likely reduces the sidewall roughness of the waveguides and consequently reduces the propagation loss. Also, the design of the feedback chip is optimized, to reduce undesired back reflections. There are no on-chip terminated waveguides anymore. In contrast to earlier designs where the through ports of the ring resonators were used as filter output, here the drop ports are used to enable better filtering. And finally, the hybrid assembly technology is developed further for stable and low-loss coupling between the gain chip and the feedback chip. The combination of these technological advances has probably brought the improved characteristics of the laser investigated here, compared to earlier versions of similar hybrid lasers.

4.2 Laser tuning response

4.2.1 Heater resistances

For accurate control of the tuning of the laser, it is required to know exactly how much phase shift is applied by each heater on the feedback chip when a certain voltage is set across this heater. The dissipated electric power in a heater is to first order linear with the temperature increase of the waveguide, which is also to first order linear with the applied phase shift. In contrast, the dissipated power is not linear with the set heater voltage. Applying a voltage U on the heater with resistance R results in a dissipated power P described by $P = \frac{U^2}{R}$. Therefore $P \sim U^2$, assuming a constant value of the resistor. However, the platinum heaters deposited on the feedback chip have a positive temperature coefficient and, therefore, the heater resistance increases with increasing temperature due to the dissipated power.

To investigate the temperature dependent resistance for the heaters used, we have electrically characterized these heaters. We measured the heater current I as function of the set heater voltage U

for the various heaters placed on the feedback circuit. The results are shown in Fig. 4.4 (a), and the temperature dependence of the heater resistance becomes apparent at the higher driving voltages. In Fig. 4.4 (b) we plot the calculated heater resistance $\frac{U}{I}$ versus the calculated heater power UI . Fig. 4.4 (b) shows that all heaters have the same power dependence of $0.050 \pm 0.002 \text{ } \Omega/\text{mW}$, but differ in nominal resistance, which can be addressed to the different length of the heaters. For instance, the length of the microring heaters is limited by the roundtrip length, which is shorter than the 1 mm length used for the other heaters.

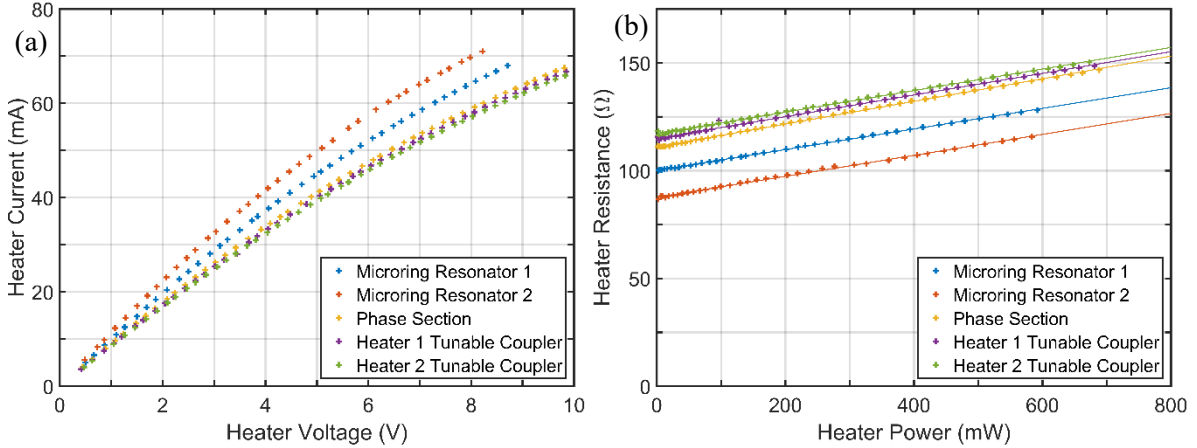


Fig. 4.4. Measured electrical response of the thermo-optic phase shifter on the feedback chip: (a) heater current vs. heater voltage and (b) calculated heater resistance vs. calculated heater power.

Regarding the temperature dependence of the heaters, it can be derived from the data in Fig. 4.4 (b) that the resistance value increases by as much as 30% at the maximum allowable heater power. This significant effect should be included in the model of these heaters, for accurate control of the laser. For this purpose, a linear fit was applied to the calculated heater resistances (Fig. 4.4 (b)) and the fit results are used in the LabVIEW program for controlling the lasers. This model, in combination with the values of the power required for 2π phase shift at each heater, $P_{2\pi}$, allows for calculating the required heater voltage as function of the applied phase shift, and vice versa. This modelling and calibration of the heaters is ultimately required for the technical realization of predictable and mode-hop-free tuning of the laser wavelength.

4.2.2 Tuning by the phase section

The most straightforward way to change the laser wavelength is via the phase section. The effect of this laser setting is to change the roundtrip phase of the laser cavity, resulting in a change of resonant cavity wavelength (*cf.* Eq. 2.11). Theoretically, by changing the heater power on the phase section, the laser wavelength can be tuned continuously over a range, limited by one FSR of the laser cavity. As a second effect, the detuning between the cavity mode and Vernier transmission peak would change the losses in the laser cavity, leading to a change of the output power as well.

To investigate the laser tuning by the phase section, we measured the wavelength and output power of the laser, when varying the electrical power on the phase section heater. To improve the detection of small wavelength steps, we used the Finisar WaveAnalyzer 1500S as OSA, because of its high resolution. The resulting measurements are shown in Fig. 4.5. Indeed, Fig. 4.5 (a) shows a continuous increase in lasing wavelength when the heater power of the phase section is increased. The tuning follows almost a linear dependence, as expected based on Eq. 2.11. Immediately after a mode hop, the tuning is slightly nonlinear, which we believe is due to a change in effective length contribution of the rings inside the laser cavity, when the cavity mode is detuned from the ring resonances. The data of Fig. 4.5 (b) recorded simultaneously show a continuous decrease in output power of the laser, when

the heater power is increased. The latter is in agreement with the initial setting of the laser, where the Vernier resonance coincides with a laser cavity mode.

The most apparent factor in Fig. 4.5 (a) and (b) is a set of discontinuities. At these points, the continuous tuning range is terminated by a mode hop for a particular heater power level corresponding to a phase shift of π . When the phase section is tuned to a multiple of π , the laser hops to larger mode numbers, with corresponding wavelength discontinuities. These mode hops limit the tuning range to the cavity FSR and cause large variations in the output power of the laser, both being highly undesired.

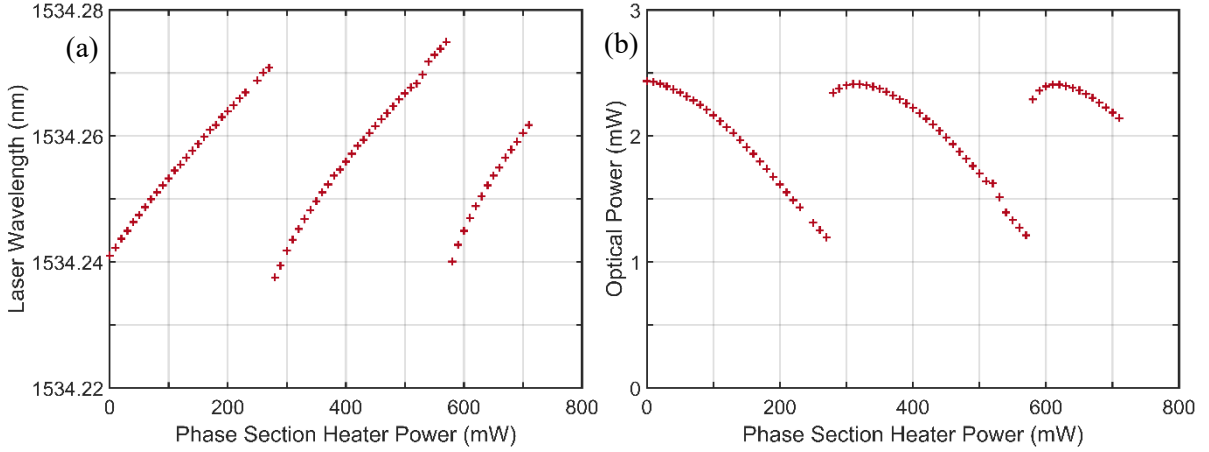


Fig. 4.5. (a) Measured wavelength and (b) output power of the laser when only the heater power on the phase section is varied. The amplifier current is 70 mA, the outcoupling set by the tunable coupler is $\sim 80\%$, and the target wavelength of the Vernier filter is set to 1534.325 nm.

From the characterization of the phase section, we can retrieve the cavity FSR, $\Delta\lambda_c$, by taking the average of the laser wavelength shifts by the mode hops. By evaluating Eq. 2.9 with this FSR and the group index of Si_3N_4 waveguides as provided in Table 3.1, an effective cavity length $L'_{\text{eff},c}$ of about 20 mm is estimated. What can also be retrieved, is the heater power $P_{2\pi,\text{ps}}$ required for 2π phase tuning, by taking the difference in heater power between two mode hops. The resulting values are shown in Table 4.1.

Tuning the laser wavelength by only changing the phase section heater power results in a very limited wavelength tuning range with variable output power, due to the relative long cavity length of 20 mm. In order to enable tuning over a much larger wavelength range while maintaining an approximately constant output power, in the next section, we describe additional tuning by the microring resonators.

Table 4.1. Experimentally retrieved parameters of the phase section for a laser wavelength around 1534 nm.

Symbol	Value	Description
$\Delta\lambda_c$	0.0341 ± 0.0008 nm	Free spectral range of the laser cavity
$L'_{\text{eff},c}$	20.1 ± 0.5 mm	Effective cavity length
$P_{2\pi,\text{ps}}$	0.58 ± 0.01 W	Heater power required for 2π phase tuning

4.2.3 Tuning by a single microring resonator

The Vernier feedback filter for the laser investigated here consists of 2 microring resonators with slightly different radii. To facilitate predictable wavelength tuning by the Vernier filter, first we investigate the tuning of the microring resonators individually. For each ring resonator, we swept the heater power and measured the laser wavelength with the peak detection algorithm of the OSA, after optimizing the laser output power via tuning of the phase section. The ANDO AQ6317 was used as OSA because it is able to measure the laser wavelength over a large range. While tuning one ring, the heater for the other ring is turned off. Results of these sweeps are shown in Fig. 4.6 (a) and (b) for the

first and second microring resonator, respectively. The highest detected peak, corresponding with the main laser mode, is shown in red. Any other detected peaks, corresponding with weaker side modes, are shown in blue. The power of these side modes varies between -34 and -57 dB with respect to the main mode.

Fig. 4.6 shows that the lasing wavelength can be tuned over a much larger range, compared to tuning by the phase section. The tuning range now corresponds to the FSR of the Vernier filter (~ 50 nm). However, it can also be seen that tuning is no longer continuous and mode hops are visible. When microring 1 is tuned, the mode hops are set by the resonances of microring 2, which are at fixed locations on the wavelength axis. Therefore, tuning only microring 1 reveals the FSR of microring 2, while tuning only microring 2 reveals the FSR of microring 1. Further, Fig. 4.6 shows opposite tuning of the laser wavelength when the heater power for microring 1 and 2 is increased, respectively. This is in agreement with microring 1 having the smaller FSR (greater roundtrip length) of the two. Finally, Fig. 4.6 shows that for wavelengths up to 1555 nm, for each lasing wavelength there is a certain heater power where no side modes are detected within the measurement range of the OSA, while for neighboring heater powers one or two side modes are present. At longer lasing wavelengths, side modes are nearly always present for the heater powers used. This is probably due to the higher gain at these wavelengths. We also conclude that careful tuning of the heater powers is required, to a higher degree than used in this experiment, for proper single mode lasing.

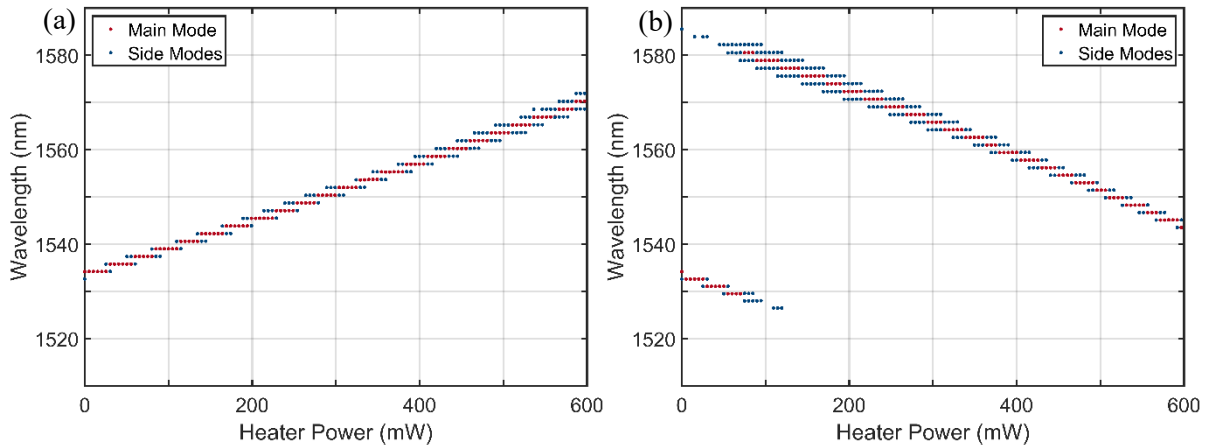


Fig. 4.6. Measured laser wavelength as function of tuning the heater powers on microring 1 (a) and microring 2 (b). The amplifier current is 50 mA, the outcoupling is set by the tunable coupler to $\sim 80\%$ and auto-phase tuning is applied for every measurement. The measured wavelengths of sidemodes in the laser spectra (blue) are indicated separately from the wavelength of the main laser mode (red).

The experimental data can be used to retrieve some parameters of the microrings, in particular the roundtrip length. Knowing these values allows more accurate simulation of the laser performance and allows for a model to more accurately predict the lasing wavelength. This is especially useful for mode-hop-free tuning and setting the laser to an arbitrary lasing wavelength.

The straightforward method to obtain the roundtrip length of the MRRs is to evaluate Eq. 2.13 for the FSR at a certain lasing wavelength. However, this method is associated with a relative large uncertainty in the obtained roundtrip length, due to the limited resolution of the OSA. To increase the certainty statistically, we calculate the roundtrip length for each detected FSR and we take the average of the calculated values. Here we use a model of the wavelength dependent group index, represented by a linear fit. The results of this processing are shown in Table 4.2. Comparison of these averaged roundtrip lengths with the corresponding design values (see Table 3.1) shows that the calculated lengths agree with the design values within the measurement uncertainty. If we assume that the coupling constants κ^2 are equal for both rings, then its value can be calculated by evaluating Eqs. 2.7 and 2.20 with the experimentally determined effective cavity length and ring resonator lengths. The resulting value, as provided in Table 4.2, is lower than the design value of 0.10. This could be

explained by a slight deviation of the waveguide width during fabrication, which changes the coupling of the light between the bus and ring waveguide. The table also shows the estimated values for the power required for 2π phase shift, $P_{2\pi,r}$. These values are obtained by extrapolation and therefore are less accurate. The reason is that applying a phase shift over 2π is not possible here, due to the heater current limit of 70 mA that we follow for the microring heaters, and the according power limit of approximately 600 mW.

Table 4.2. Experimentally retrieved parameters of the Vernier filter, given at a wavelength of 1534 nm.

Symbol	Value	Description
$\Delta\lambda_{r1}$	1.547 ± 0.001 nm	Free spectral range of MRR 1
$\Delta\lambda_{r2}$	1.597 ± 0.002 nm	Free spectral range of MRR 2
$L_{rt,r1}$	885 ± 1 μ m	Roundtrip length of MRR 1
$L_{rt,r2}$	857 ± 1 μ m	Roundtrip length of MRR 2
κ^2	0.071 ± 0.003	Power coupling coefficient between bus and MRR
$P_{2\pi,r1}$	0.78 ± 0.01 W	Heater power required for 2π phase tuning of MRR 1
$P_{2\pi,r2}$	0.75 ± 0.01 W	Heater power required for 2π phase tuning of MRR 2

By using the measured values, the transmission function of the Vernier filter can be simulated, which corresponds to a calibration of wavelength changes versus heater current. However, due to a remaining uncertainty in the order of 1 μ m in the roundtrip length, this model is not sufficiently accurate to predict the absolute wavelength for zero tuning, *i.e.*, with all heaters off. For instance, based on the nominal measured roundtrip lengths, the predicted zero-tuning wavelength is 1525.6 nm, while the measured value is 1534.2 nm. Due to the small roundtrip length difference between the two rings, this zero-tuning wavelength is very sensitive to the actual length difference between these rings. Nevertheless, to attempt to achieve agreement between model and measurement, we tweak the found ring lengths until the predicted zero-tuning wavelength agrees with the measured value. Indeed, after tweaking, the roundtrip lengths of 885.6 and 857.7 μ m for microring 1 and 2, respectively, provide the measured zero-tuning wavelength and are still within the measurement uncertainty of the experimentally retrieved values.

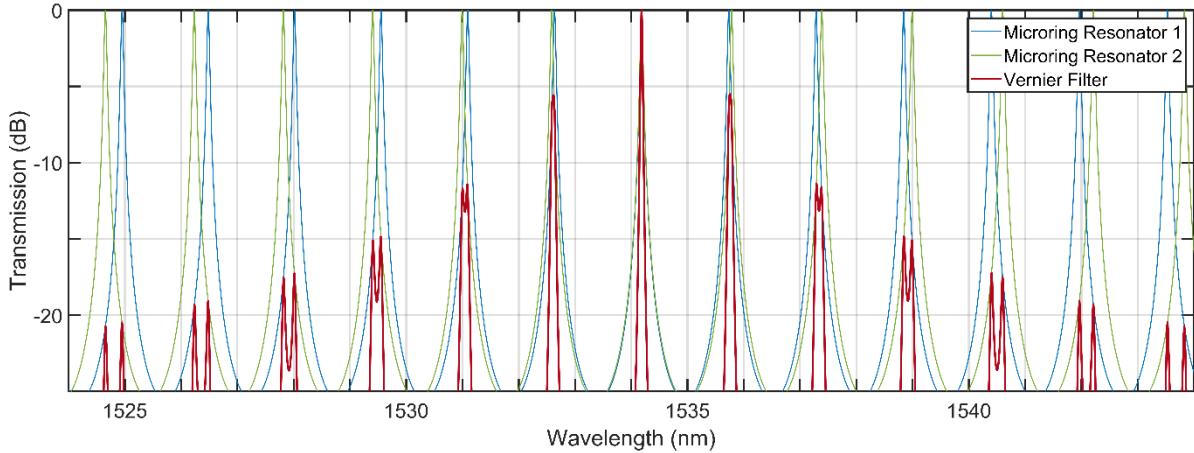


Fig. 4.7. Modelled transmission of both ring resonators and the Vernier filter, for power coupling coefficients $\kappa^2 = 0.1$ and assuming no losses. When the heaters on both ring resonators are not actuated, maximum transmission is approximately at 1534.1 nm, which corresponds with the zero-tuning wavelength of the laser.

The simulated transmission function of the Vernier filter, based on the tweaked roundtrip values for both ring resonators, is shown in Fig. 4.7. The transmission peak around 1534.1 nm is approximately the zero-tuning laser wavelength (*cf.* Fig. 4.6). By adding the phase shift, applied by microring heaters, into this model, the transmission function can be predicted when setting the heaters to any value. The reverse calculation, namely setting the heaters as function of a requested wavelength is

then also possible. Such a model was implemented into the LabVIEW program for controlling the laser, to enable predictable wavelength tuning of the laser within the FSR of the Vernier filter.

To summarize what has been presented so far, we have described how the laser wavelength can be accurately predicted, based on a calibrated model of the Vernier filter. We have demonstrated that the laser wavelength can be adjusted continuously over a small range, limited by mode hops, by tuning the phase section or with mode hops over a larger range by tuning the ring resonators. In the next chapter we will show how to use these elements together in a suitable synchronism for tuning over a large range, not limited by mode hops.

4.3 Mode-hop-free tuning

For continuous wavelength tuning of the laser, *i.e.*, avoiding mode hops, over a range larger than the cavity FSR, we investigate here laser tuning via synchronous variation of the Vernier filter and phase section. By tuning both ring resonators together, not only does the Vernier filter transmission peak shift continuously, but also the resonant laser wavelength changes, as we derive in section 2.4.

However, these wavelength shifts are clearly not equal, due to the presence of non-tuned parts in the circuit, specifically the bus waveguides and the optical amplifier. Therefore, also a tuning of the phase section is required, to keep the shift of the laser cavity mode equal to the shift of the resonant wavelength of the Vernier filter.

The challenge with tuning all these three elements together is to find the right tuning ratios of the heater powers and corresponding phase shifts for all the elements, that synchronize Vernier filter and cavity length tuning. In section 2.6 we derived this tuning ratio theoretically. However, as these expressions were not available at the time of performing the experiment, the ratios were determined experimentally.

The approach we used was to first align the Vernier filter resonance to a resonance of the laser cavity. This was done by tuning the Vernier filter, without applying any heater power to the phase section, and maximize the output during tuning. This resulted in an initial wavelength of 1534.25 nm. In this way the full heater power range of the phase section remains available for tuning the laser. Next, we optimized the tuning ratio between the phase section and the Vernier filter, by maximizing the laser output power during synchronous tuning and by rejecting a tuning ratio if an undesired mode hop occurred. The ratios $\frac{\partial\phi_{r1}}{\partial\phi_{ps}} = 0.107$ and $\frac{\partial\phi_{r2}}{\partial\phi_{ps}} = 0.103$ for ring resonator 1 and 2, respectively, were found experimentally to provide the maximum laser power during synchronous tuning. For comparison, the theoretical values obtained from Eq. 2.41, using the laser parameters from Tables 4.1 and 4.2, are $\frac{\partial\phi_{r1}}{\partial\phi_{ps}} = 0.108$ and $\frac{\partial\phi_{r2}}{\partial\phi_{ps}} = 0.105$, for ring resonator 1 and 2, respectively, agree closely with the experimental values. Using the experimentally optimized tuning ratios, we chose discrete values of heater powers to tune the laser wavelength in 0.005 nm intervals. The required heater power for the ring resonators as a function of the heater power for the phase section are shown in Fig. 4.8 (a) as blue and red data points for rings 1 and 2, respectively. After each interval of tuning, *i.e.*, after applying each set of heater powers to the phase section and ring resonators, a laser spectrum was acquired, using the Finisar WaveAnalyzer 1500S, and the laser output power was measured. The measured spectra are shown superimposed in Fig. 4.8 (b), while the corresponding laser center wavelengths and laser output powers are shown in Fig. 4.8 (c, red) and Fig. 4.8 (d, red), respectively. For comparison, Fig. 4.8 (c, blue) also shows the lasing wavelength and Fig. 4.8 (d, blue) shows the output power, when only the phase section is tuned and the heater power for the two rings is kept constant.

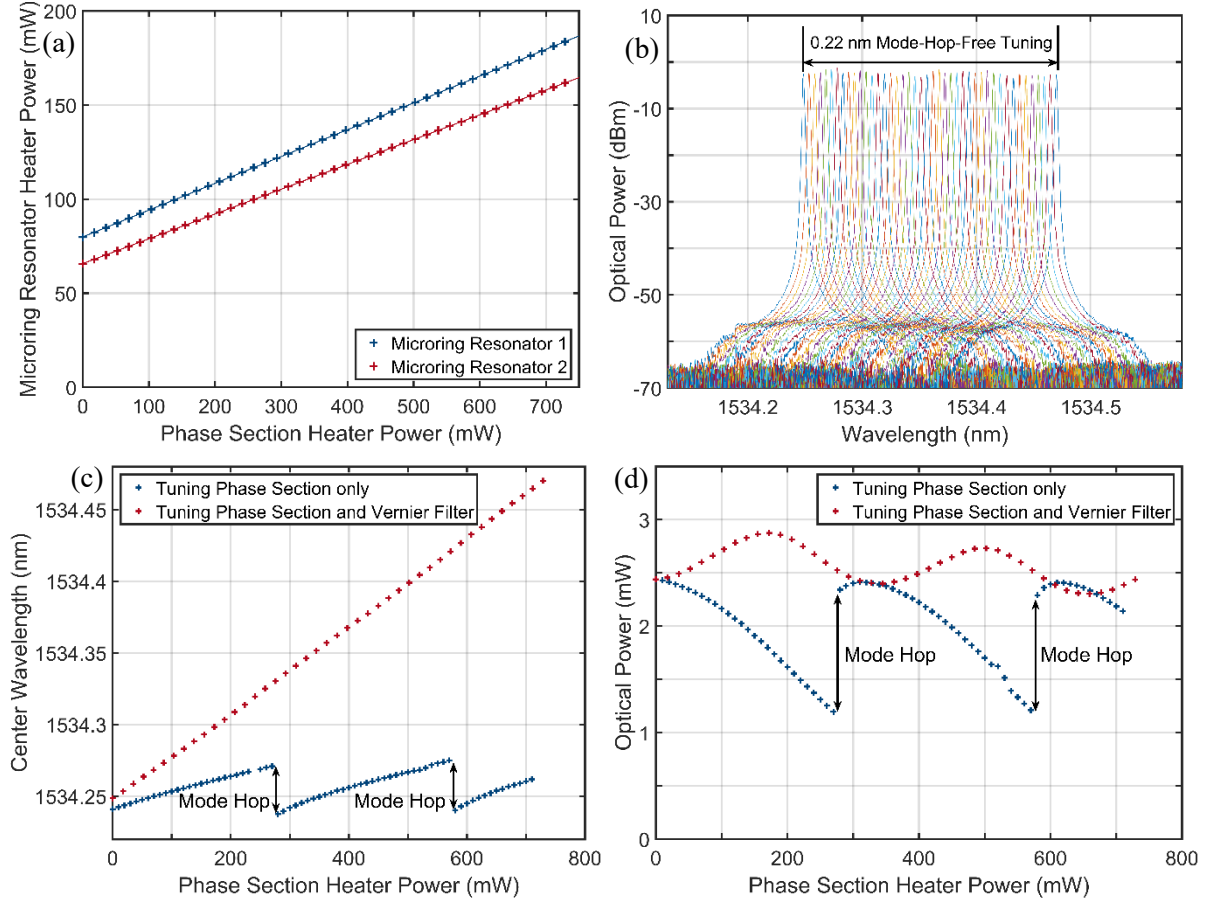


Fig. 4.8. (a) Experimentally optimized heater power tuning ratios between the phase section and the ring resonators for synchronous tuning. The shown datapoints are calculated for a tuning interval of 0.005 nm. (b) Superimposed OSA spectra, taken with an interval of 0.005 nm, for synchronous tuning of phase section with the Vernier filter, which demonstrates the 0.22 nm mode-hop-free tuning range. (c) Measured laser wavelength and (d) output power as function of the phase section heater power. Synchronous tuning of the phase section with the Vernier filter is shown by the red data points, while the tuning of only the phase section is shown by the blue data points for comparison. Mode hops are only visible in the latter measurement series. The amplifier current is 70 mA and the outcoupling set by the tunable coupler is $\sim 80\%$ for these measurements.

Fig. 4.8 (c) and (d) clearly display the difference between synchronous tuning and tuning of the phase section alone. For the latter, mode hops are clearly visible as discontinuities in lasing wavelength and output power. On the other hand, synchronous tuning provides a continuous wavelength tuning. Also, a stable output power is observed due to the absence of power discontinuities over a much larger range. Although we aimed for a constant output power, Fig. 4.8 (d, red) shows a small remaining oscillation in optical power with a period that seems to correspond to the distance between the mode hops. This may indicate that the oscillation is due to a non-optimal setting of one or more of the tuning parameters of the laser, which modulates the laser losses when the laser cavity is tuned synchronously with the Vernier filter.

Fig. 4.8 (c) further shows an interesting effect. In a standard external cavity diode laser, *e.g.* in a Littrow configuration, one expects that synchronous tuning the filter (grating) with a phase section yields a wider tuning range than one cavity FSR, but that the tuning slope remains unchanged. However, we observe also a steeper tuning slope, *i.e.*, a higher tuning sensitivity. The tuning slope of laser wavelength versus phase section heater power is found to be 0.31 pm/mW for synchronous tuning, while it is only 0.11 pm/mW when only the heater power of the phase section is varied. Synchronous tuning has increased the tuning sensitivity by a factor of 2.8. This effect is confirmed to be present also from the theoretical analysis. From Eqs. 2.11 and 2.39 we expect a tuning sensitivity increase factor of 2.5 using the experimental values of Table 4.1 and Table 4.2. The observed

increased tuning slope confirms the tuning model described in chapter 2, where we attribute this increase by the change of cavity resonant wavelength due to heating the ring resonators, which is enhanced by the multiple passes that the light performs through the ring resonators. The synchronous tuning results in a tuning sensitivity of this laser as if the rings are not present, *i.e.*, as if the laser possesses a much shorter cavity. In addition, synchronous tuning allows a larger added phase than π by the phase section without inducing a mode hop due to the equal wavelength shifts of the Vernier filter transmission and the lasing cavity mode.

Most importantly, Fig. 4.8 (b) and (c) show that the continuous wavelength tuning range of the laser is significantly increased to 0.22 nm when using synchronous tuning of the heaters. This wavelength range is approximately 6 times the cavity FSR, which limits the tuning when only the phase section is used. Both the absence of mode hops and the increased tuning sensitivity result in this significant increase. The continuous tuning range we realized with this laser is technically limited by the maximum heater power of approximately 730 mW that can be applied to the phase section. Therefore, Eq. 2.42 is appropriate in determining the maximum continuous or mode-hop-free tuning range. This equation gives a tuning range of 0.21 nm, when using the maximum phase shift by the phase section of 2.5π and the experimental laser parameters of Table 4.1 and Table 4.2. The calculated value agrees well with the experimentally found range. The overall good agreement between the experimentally determined tuning properties and the analytical model of chapter 2 demonstrates again that the laser tuning model provides an accurate description of our mode-hop-free tuning method.

4.4 Acetylene absorption spectroscopy with mode-hop-free laser tuning

4.4.1 Acetylene absorption spectrum

In the previous section we demonstrated mode-hop-free tuning of the laser. The capability to tune a narrow laser line continuously over a certain wavelength range suggests that such a laser can be used for high-resolution spectroscopy without the need of a separate wavelength meter. We demonstrate this by measuring several of the absorption lines of acetylene. Acetylene is chosen because it has a well-known absorption spectrum in the range of interest that can be accurately calculated using the HITRAN spectroscopic database^[43]. By comparing our measurements with the HITRAN based absorption spectrum, we verify that the laser can be swept continuously over the wavelength range of the absorption lines.

Acetylene ($^{12}\text{C}_2\text{H}_2$) is a small gas molecule consisting of only two carbon and two hydrogen atoms. Due to the low number of atoms, the absorption spectrum shows a relatively simple structure. The spectrum in the range between 1510 and 1540 nm contains about 50 strong and well-defined absorption lines. These lines are due to transitions involving changes in both vibrational and rotational states of the molecule, also called ro-vibrational transitions, where a change in quantum rotational number ΔJ equal to $\Delta J = +1$ corresponds to the so-called *R*-branch and $\Delta J = -1$ corresponds to the so-called *P*-branch^[46]. The rotational levels, which are much closer spaced than the vibrational levels, give a fine sub-structure to the vibrational transition. This transition is associated with the $\nu_1 + \nu_3$ vibrational combination band, based on the simultaneous excitation of the symmetric (ν_1) and the asymmetric (ν_3) C-H stretch.

Fig. 4.9 (a) shows a recorded acetylene spectrum in the wavelength region of interest, measured with spectrally broadband light from a LED, passed through an acetylene-filled absorption cell^[44]. To simulate the absorption spectrum based on the spectroscopic data from the HITRAN database, depending on the gas cell temperature, pressure and length, several applications are available, including SpectraPlot^[45]. We used this tool to calculate the absorption spectrum as shown in Fig. 4.9 (b), with similar experimental conditions as the recorded spectrum in Fig. 4.9 (a). The comparison of both graphs clearly shows that the measured and calculated absorption spectra are in good agreement.

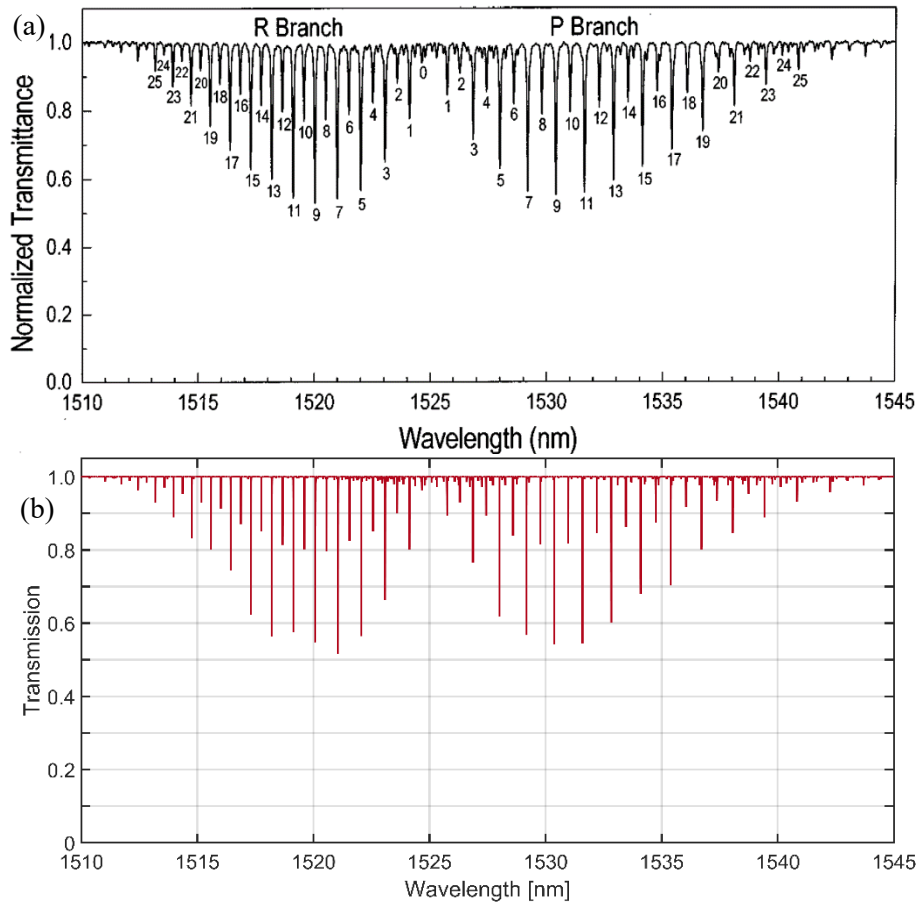


Fig. 4.9. (a) Acetylene ($^{12}\text{C}_2\text{H}_2$) spectrum taken by passing light from a LED through a 5 cm long absorption cell and recording the spectrum of the transmitted light with an OSA. This spectrum has been normalized to the LED spectrum^[44]. (b) Simulated acetylene spectrum with SpectraPlot^[45], under similar environmental conditions as the measured spectrum, namely $T = 295$ K, $P = 0.08$ atm and $L = 5$ cm.

4.4.2 Wavelength sweep over an acetylene absorption line

To measure the acetylene absorption lines by applying the mode-hop-free tuning to our hybrid laser, we use an experimental setup as shown schematically in Fig. 4.10. The output fiber of the laser is connected with a fiber isolator (Thorlabs IO-G-1550-APC) to reduce unwanted external reflections back into the laser. The output light is then equally divided by a 50:50 fiber optic coupler (Thorlabs TW1550R5A2) over two outputs. One part is sent through the acetylene gas cell to a photodiode (Thorlabs S144C), while the other part serves as a reference. This reference is again split in two by a 95:5 fiber optic coupler (AOFR WBY05131510aSR). The largest part is sent to a second equivalent photodiode, while the remaining 5% is used to check the wavelength of the laser with an optical spectrum analyzer (Ando AQ6317). The acetylene gas cell is a standard sealed fiber-coupled package from Wavelength Reference Inc., with a path length of 5.5 cm and a pressure of 50 ± 5 Torr. This cell was held at the lab temperature of about 295 K.

To record transmission spectra, the laser was mode-hop-free tuned over a range of ~ 0.2 nm with a step size of ~ 0.1 pm. As the step size is much smaller than the resolution of the OSA, which is 15 pm, the set-value of the laser was measured with the OSA for about 100 different set-values along the range. Linear interpolation is then used to convert the range of set-values into wavelength. For the various scans performed, the linear interpolations have coefficients of determination equal to or better than 0.9988 , showing a very linear relation between set-values and wavelengths measured by the OSA. As this calibration still may contain a systematic error, *e.g.*, the OSA has a fixed offset in

wavelength, we decided to offset each of the measured absorption lines to coincide with the corresponding calculated absorption lines.

The acetylene absorption was retrieved from dividing the signal from photodiode PD1 (see Fig. 4.10) by the reference photodiode PD2 to remove any intensity fluctuations from the laser. The result is then normalized to the maximum signal as measured by reference photodiode PD2, in order to allow a direct comparison between the measured and calculated absorption line shapes.

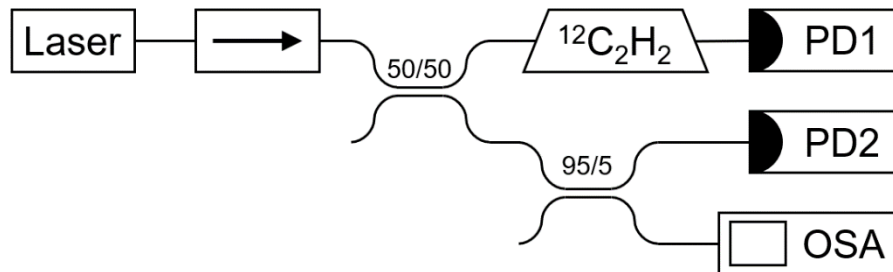


Fig. 4.10. Schematic view of the experimental set-up for the acetylene absorption measurement, showing the laser, an isolator (\rightarrow), a 50/50 fiber optic coupler, a 95/5 fiber optic coupler, the acetylene ($^{12}\text{C}_2\text{H}_2$) absorption cell, two photodiodes (PD1 and PD2) and the optical spectrum analyzer (OSA).

The measured traces are plotted in Fig. 4.11 (a) to (c) for absorption lines P13, P19 and P21, respectively. Also shown is the calculated normalized transmission as calculated with SpectraPlot^[45] based on HITRAN data. The manufacturer specifications of the acetylene gas cell are used as input parameters for the calculated transmission. The offsets applied to each of the measured absorption lines, are -15.4 pm, -1.8 pm, and -5.7 pm for the P13, P19 and P21 lines, respectively. The average offset of -7.6 pm with a standard deviation of 5.7 pm falls well within the resolution of the OSA.

We observe in Fig. 4.11 an overall good match between our measured and the predicted transmission. However, a slight mismatch could be observed between the measured and predicted traces. The measured absorption lines are slightly broader and stronger than the calculated lines. We address this mismatch in part to the uncertainty in gas cell pressure and in part to the uncertainty in calibration of the laser wavelength. Especially, the latter may be responsible for the slight misalignment of the secondary absorption lines in the measured spectrum compared to the calculated spectrum. The measured acetylene absorption demonstrates clearly that the laser could be tuned mode-hop-free over a range of ~ 0.23 nm (~ 29 GHz) with a step size as small as ~ 0.12 pm (~ 15 MHz).

Although the laser is capable of tuning its wavelength over absorption lines P13, P19 and P21 with high accuracy, it was not possible to measure all of the absorption lines. The reason is that the heaters on the microring resonators do not support full 2π phase tuning. As a result, certain wavelengths cannot be set with fine-tuning of the Vernier filter, and a wavelength sweep over several other absorption lines is not possible. We expect that the support of full 2π phase tuning for the heaters will ensure measurement of all absorption lines with very high resolution. Also, the minimum wavelength step size for the laser depends nonlinearly on the actual wavelength setting of the laser, by using the control electronics as described in section 3.2. Any requested DAC value is almost linearly converted to a heater voltage, but the corresponding heater power and laser wavelength tuning depend approximately quadratically on the DAC value. A linear control of the heater power would enable a fixed wavelength step size over the tuning range of the laser.

Finally, we like to point out that acetylene is an excellent choice for a wavelength reference at telecom wavelengths. Its ground state has zero angular momentum of the electron cloud and the molecule has no permanent electric dipole due to its symmetry. The main source of line shift is due to an energy-level shift caused by elastic collisions and is thus pressure dependent. These properties make the molecule particularly insensitive to external perturbations caused by temperature fluctuations or by an electromagnetic field^[44]. Indeed, the long-term frequency stability was improved

to a level of $\sim 10^{-12}$ and a reproducibility of ~ 10 kHz by locking a semiconductor laser to various acetylene absorption lines^[17]. For precise wavelength stabilization of the laser, it is required to use narrow and strong acetylene absorption lines. Therefore, an acetylene cell with a lower gas pressure and a longer length would be more suitable for laser locking than the gas cell used for this experiment. The hybrid extended cavity diode laser investigated here has a mode-hop-free tuning range that is wide enough to safely tune across an individual absorption line, including possible side peaks. In addition, it allows for very small changes in the wavelength. Therefore, it is an ideal candidate for wavelength stabilization and locking to, *e.g.*, the wing of an acetylene absorption line. This would be beneficial to various applications including high precision laser-based metrology.

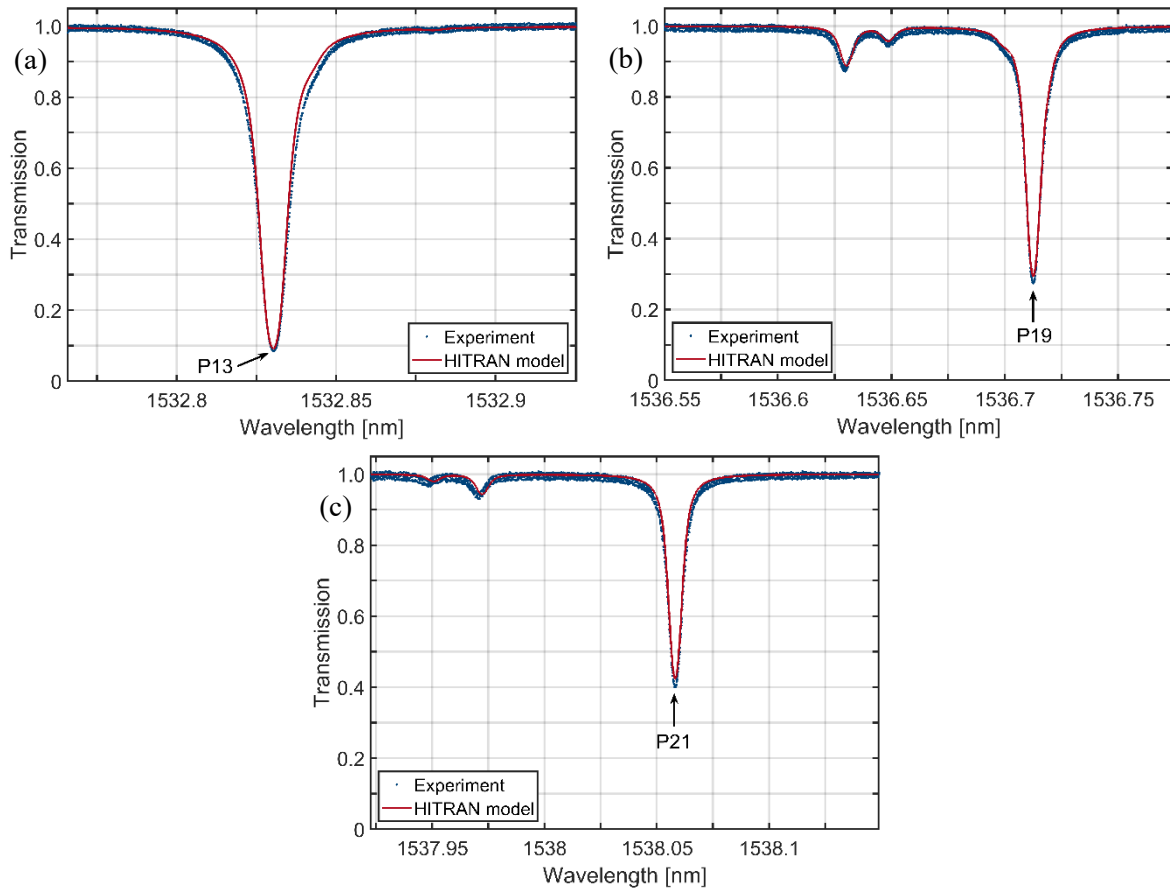


Fig. 4.11. Measured and modelled transmission through an acetylene gas cell as function of wavelength for different absorption lines (a) P13 at $\lambda = 1532.830$ nm, (b) P19 at $\lambda = 1536.713$ nm, and (c) P21 at $\lambda = 1538.058$ nm. The modelled transmission assumes a temperature of 295 K, and a gas cell with 5.5 cm length and 50 Torr pressure.

5 Conclusions and outlook

We present in this thesis for the first time on-chip, all-electronic and mode-hop-free wavelength tuning of an integrated extended-cavity laser with a tuning range that extends beyond its standard mode spacing limit. The hybrid laser used here comprises an InP amplifier and a Si₃N₄ waveguide-based frequency selective feedback circuit with a tunable phase section and two tunable microring resonators in a Vernier configuration. This long and low-loss cavity enables a narrow Schawlow-Townes laser linewidth, for this particular laser in the order of 10 kHz. However, the long cavity also reduces the cavity mode spacing, which forms the standard limit for continuous wavelength tuning. We present a synchronous tuning method of the phase section with the microrings to enable both a large continuous tuning range and a narrow Schawlow-Townes linewidth for a chip-based laser. Furthermore, we provide for the first time an analytical model for this synchronous tuning method and validated it with experimental data.

We experimentally demonstrated that tuning the laser with only the phase section results in a mode-hop-free wavelength tuning range equal to the standard free spectral range of the laser cavity, which is 0.034 nm. Further tuning, beyond an induced phase of π , results in mode hops, visible as discontinuities in both the laser wavelength and output power. Synchronous control of the phase section and both microring resonators with the proper ratio avoids these mode hops and has the added advantage of a higher tuning sensitivity, *i.e.*, a larger shift in laser wavelength for a given change in induced phase by the phase section. With synchronous control, we demonstrated continuous wavelength tuning over a much larger range of 0.22 nm, which is larger by a factor of 6 compared to tuning by the phase section only. Both, the larger tuning sensitivity as well as the larger tuning range are due to the additional and synchronous tuning of the microrings present in the laser resonator. The phase added to the light inside the rings, not only shifts the ring transmission peak, but also adds phase to the light inside the laser cavity, which is enhanced by the multiple passes that the light performs through the rings. This effect yields the increased tuning sensitivity, while the transmission filter shift prevents mode hops and allows an increased tuning range.

An analytical model describing the mode-hop-free tuning of the hybrid laser has been developed. As is well-known, for determining the Schawlow-Townes linewidth of the laser, the full cavity length, including the effective length of the microring resonators, needs to be taken into account. On the other hand, the tuning model shows that for the mode-hop-free tuning of the laser, the effective length of the microring resonators can be excluded from the cavity length, provided that the phase section and microring resonators are controlled synchronously in the appropriate way. Good agreement was found between predictions based on this model with experimental data.

The tuning model allows, after appropriate calibration, to accurately predict the lasing wavelength for given laser settings. To demonstrate this and the mode-hop-free tuning, we performed an acetylene transmission measurement with wavelength steps of ~ 0.12 pm (~ 15 MHz) for several absorption lines. Good agreement was found between the result and the calculated absorption spectrum using the HITRAN database, showing accurate, high-resolution and mode-hop-free tuning of the hybrid laser.

To remove some of the current limitations of the investigated hybrid laser, several modifications are suggested. First, the Vernier FSR of 50.5 nm around the nominal wavelength of 1550 nm should be increased to at least 120 nm to cover the full gain bandwidth. This will considerably simplify the wavelength tuning of the laser and prevent the laser to become multimode with modes spaced at the Vernier FSR. Second, the heaters for the microring resonators are unable to induce an optical phase shift of 2π for a single roundtrip of the light in the ring. As a result, certain wavelengths cannot be set with fine-tuning the Vernier filter. To ensure complete wavelength coverage of the laser, full 2π -phase tuning should be guaranteed, either by a slight increase of the circumference of the rings or by more effective phase shifting elements. Third, to enable wavelength tuning with fixed small step sizes,

a linear control of the dissipated power in the heaters would be required, instead of the current linear control of heater voltages by the DACs on the PCB. Finally, operation of the laser would greatly benefit from on-chip detectors for the optical power^[47] and for the gain voltage^[48]. These signals could enable optimization algorithms for laser settings and provide the best laser performance, *e.g.*, allow continuous tuning of the laser wavelength at truly constant output power.

To further increase the mode-hop-free tuning range, we suggest the following improvements. The tuning range is in the current design limited by the optical phase induced by the phase section. Thus, a larger part of bus waveguides needs to be converted to a phase section by covering it with a heater. The length of the remaining, unheated bus waveguide should be minimized. To increase the effectiveness of the thermal heaters, the top cladding thickness could be reduced to the minimum value that does not affect the optical propagation loss. We estimate that these suggested improvements will increase the mode-hop-free tuning range to a value between 1 and 2 nm for this hybrid laser type. In addition, the Schawlow-Townes linewidth could be further reduced, without reducing the mode-hop-free tuning range. For this purpose, a microring configuration could be implemented where each ring is passed twice on every cavity roundtrip, instead of the current configuration where the rings are placed in a loop mirror. The rings could also have weaker coupling to the bus waveguides. This enhances the effective length of the rings and thus lowers the Schawlow-Townes linewidth. According to our model, this would not affect mode-hop-free tuning of the hybrid laser.

The advantages of the presented mode-hop-free tuning approach can be further exploited with other laser designs. A VCSEL typically has a much shorter gain length than the edge-emitting amplifier used in the current design, which is beneficial for obtaining a large tuning sensitivity. Coupling a VCSEL to an external cavity based on tunable microring resonators could benefit from the same linewidth reduction and mode-hop-free tuning approach, as described in this thesis, to possibly outperform the hybrid laser investigated here. Moving the phase section to the SOA chip may provide a more effective phase shifter resulting in a larger phase shift over a smaller length. Also, replacing the resistive heaters with novel types of phase shifters would offer several benefits. Stress-optic tuning by PZT phase shifters can reduce the power consumption with two orders of magnitude with respect to thermal phase shifters, while enabling modulation frequencies of at least 10 kHz^[49]. Novel plasmonic modulators feature modulation beyond 500 GHz with a length of below 25 μm ^[50]. Using these faster and more effective phase shifters is advantageous for the tuning range, tuning speed and power consumption.

To conclude, the demonstrated large mode-hop-free tuning range and small Schawlow-Townes linewidth of the hybrid extended-cavity laser based on microring resonators, together with the potential for significant improvements, provides a promising, fully integrated solution that would greatly benefit applications that rely on these characteristics.

6 References

- [1] J. P. Gordon, H. J. Zeiger, and C. H. Townes, “Molecular Microwave Oscillator and New Hyperfine Structure in the Microwave Spectrum of NH₃,” *Phys. Rev.*, vol. 95, no. 1, pp. 282–284, 1954.
- [2] T. H. Maiman, “Stimulated Optical Radiation in Ruby,” *Nature*, vol. 187, no. 4736, pp. 493–494, 1960.
- [3] A. Einstein, “Zur Quantentheorie der Strahlung,” *Phys. Zeitschrift*, vol. 18, pp. 121–128, 1917.
- [4] R. N. Hall, G. E. Fenner, J. D. Kingsley, T. J. Soltys, and R. O. Carlson, “Coherent Light Emission From GaAs Junctions,” *Phys. Rev. Lett.*, vol. 9, no. 9, pp. 366–368, 1962.
- [5] S. L. I. Olsson, J. Cho, S. Chandrasekhar, X. Chen, P. J. Winzer, and S. Makovejs, “Probabilistically shaped PDM 4096-QAM transmission over up to 200 km of fiber using standard intradyne detection,” *Opt. Express*, vol. 26, no. 4, pp. 4522–4530, 2018.
- [6] ITU-T, “Spectral grids for WDM applications: DWDM frequency grid,” *Recomm. ITU-T*, no. G.694.1, 2012.
- [7] C. E. Wieman and L. Hollberg, “Using diode lasers for atomic physics,” *Rev. Sci. Instrum.*, vol. 62, no. 1, pp. 1–20, 1991.
- [8] B. Stern, X. Ji, Y. Okawachi, A. L. Gaeta, and M. Lipson, “Battery-operated integrated frequency comb generator,” *Nature*, vol. 562, pp. 401–405, 2018.
- [9] M.-G. Suh, Q.-F. Yang, K. Y. Yang, X. Yi, and K. J. Vahala, “Microresonator soliton dual-comb spectroscopy,” *Science*, vol. 354, no. 6312, pp. 600–603, 2016.
- [10] M. G. Allen, “Diode laser absorption sensors for gas-dynamic and combustion flows,” *Meas. Sci. Technol.*, vol. 9, no. 4, pp. 545–562, 1998.
- [11] L. Tombez, E. J. Zhang, J. S. Orcutt, S. Kamapurkar, and W. M. J. Green, “Methane absorption spectroscopy on a silicon photonic chip,” *Optica*, vol. 4, no. 11, pp. 1322–1325, 2017.
- [12] K. Meiners-Hagen, R. Schödel, F. Pollinger, and A. Abou-Zeid, “Multi-Wavelength Interferometry for Length Measurements Using Diode Lasers,” *Meas. Sci. Rev.*, vol. 9, no. 1, pp. 16–26, 2009.
- [13] Z. L. Newman *et al.*, “Architecture for the photonic integration of an optical atomic clock,” *Optica*, vol. 6, no. 5, pp. 680–685, 2019.
- [14] D. Marpaung, J. Yao, and J. Capmany, “Integrated microwave photonics,” *Nat. Photonics*, vol. 13, no. 2, pp. 80–90, 2019.
- [15] J. Buus, M.-C. Amann, and D. J. Blumenthal, *Tunable Laser Diodes and Related Optical Sources*, 2nd ed. Wiley, 2005.
- [16] A. L. Schawlow and C. H. Townes, “Infrared and Optical Masers,” *Phys. Rev.*, vol. 112, no. 6, pp. 1940–1949, 1958.
- [17] M. de Labachellerie, K. Nakagawa, Y. Awaji, and M. Ohtsu, “High-frequency-stability laser at 1.5 μm using Doppler-free molecular lines,” *Opt. Lett.*, vol. 20, no. 6, pp. 572–574, 1995.
- [18] K. Liu and M. G. Littman, “Novel geometry for single-mode scanning of tunable lasers,” *Opt. Lett.*, vol. 6, no. 3, pp. 117–118, 1981.
- [19] P. McNicholl and H. J. Metcalf, “Synchronous cavity mode and feedback wavelength scanning

- in dye laser oscillators with gratings,” *Appl. Opt.*, vol. 24, no. 17, pp. 2757–2761, 1985.
- [20] K. Kasai, M. Nakazawa, Y. Tomomatsu, and T. Endo, “15 μ m, mode-hop-free full C-band wavelength tunable laser diode with a linewidth of 8 kHz and a RIN of –130 dB/Hz and its extension to the L-band,” *Opt. Express*, vol. 25, no. 18, pp. 22113–22124, 2017.
- [21] B. Liu, A. Shakouri, and J. E. Bowers, “Passive microring-resonator-coupled lasers,” *Appl. Phys. Lett.*, vol. 79, no. 22, pp. 3561–3563, 2001.
- [22] B. Liu, A. Shakouri, and J. E. Bowers, “Wide tunable double ring resonator coupled lasers,” *IEEE Photonics Technol. Lett.*, vol. 14, no. 5, pp. 600–602, 2002.
- [23] R. M. Oldenbeuving, E. J. Klein, H. L. Offerhaus, C. J. Lee, H. Song, and K.-J. Boller, “25 kHz narrow spectral bandwidth of a wavelength tunable diode laser with a short waveguide-based external cavity,” *Laser Phys. Lett.*, vol. 10, no. 1, 015804, 2013.
- [24] Y. Fan *et al.*, “Optically Integrated InP–Si₃N₄ Hybrid Laser,” *IEEE Photonics J.*, vol. 8, no. 6, 1505111, 2016.
- [25] Y. Lin *et al.*, “Characterization of Hybrid InP-TriPleX Photonic Integrated Tunable Lasers Based on Silicon Nitride (Si₃N₄/SiO₂) Microring Resonators for Optical Coherent System,” *IEEE Photonics J.*, vol. 10, no. 3, 1400108, 2018.
- [26] Y. Fan *et al.*, “290 Hz Intrinsic Linewidth from an Integrated Optical Chip-based Widely Tunable InP-Si₃N₄ Hybrid Laser,” in *Conference on Lasers and Electro-Optics*, 2017, p. JTh5C.9.
- [27] T. Komljenovic *et al.*, “Widely-Tunable Ring-Resonator Semiconductor Lasers,” *Appl. Sci.*, vol. 7, no. 7, 732, 2017.
- [28] L. Wang and J.-J. He, “Single-electrode-tuned mode-hop-free tunable laser based on ring coupled cavity,” *Opt. Express*, vol. 17, no. 22, pp. 19940–19946, 2009.
- [29] C. K. Madsen and J. H. Zhao, *Optical Filter Design and Analysis: A Signal Processing Approach*, 1st ed. Wiley, 1999.
- [30] J. Buus, M.-C. Amann, and D. J. Blumenthal, *Tunable Laser Diodes and Related Optical Sources*, 2nd ed. Wiley, 2005.
- [31] R. G. Hunsperger, *Integrated Optics*, 6th ed. New York: Springer, 2009.
- [32] E. A. J. Marcatili, “Dielectric Rectangular Waveguide and Directional Coupler for Integrated Optics,” *Bell Syst. Tech. J.*, vol. 48, no. 7, pp. 2071–2102, 1969.
- [33] D. G. Rabus, *Integrated Ring Resonators*, Springer Series in Optical Sciences vol. 127. Berlin, Heidelberg: Springer, 2007.
- [34] K. Oda, N. Takato, and H. Toba, “A wide-FSR waveguide double-ring resonator for optical FDM transmission systems,” *J. Light. Technol.*, vol. 9, no. 6, pp. 728–736, 1991.
- [35] P. Dong, Y.-K. Chen, G.-H. Duan, and D. T. Neilson, “Silicon photonic devices and integrated circuits,” *Nanophotonics*, vol. 3, no. 4–5, pp. 215–228, 2014.
- [36] K. A. Williams *et al.*, “InP photonic circuits using generic integration,” *Photonics Res.*, vol. 3, no. 5, pp. B60–B68, 2015.
- [37] P. Muñoz *et al.*, “Silicon Nitride Photonic Integration Platforms for Visible, Near-Infrared and Mid-Infrared Applications,” *Sensors*, vol. 17, no. 9, 2088, 2017.
- [38] D. de Felipe *et al.*, “Polymer-Based External Cavity Lasers: Tuning Efficiency, Reliability, and Polarization Diversity,” *IEEE Photonics Technol. Lett.*, vol. 26, no. 14, pp. 1391–1394, 2014.

- [39] C. G. H. Roeloffzen *et al.*, “Low-Loss Si₃N₄ TriPleX Optical Waveguides: Technology and Applications Overview,” *IEEE J. Sel. Top. Quantum Electron.*, vol. 24, no. 4, 4400321, 2018.
- [40] Y. Fan, “Semiconductor-glass waveguide hybrid lasers with ultra-high spectral purity,” PhD thesis, University of Twente, Enschede, The Netherlands, 2017.
- [41] Y. Fan *et al.*, “A hybrid semiconductor-glass waveguide laser,” in *Proc. SPIE, Laser Sources and Applications II*, 91351B, 2014.
- [42] A. Leinse *et al.*, “Hybrid interconnection of InP and TriPleX photonic integrated circuits for new module functionality,” in *Proc. SPIE 10924, Optical Interconnects XIX*, 109240B, 2019.
- [43] L. S. Rothman *et al.*, “The HITRAN2012 molecular spectroscopic database,” *J. Quant. Spectrosc. Radiat. Transf.*, vol. 130, pp. 4–50, 2013.
- [44] W. C. Swann and S. L. Gilbert, “Pressure-induced shift and broadening of 1510–1540-nm acetylene wavelength calibration lines,” *J. Opt. Soc. Am. B*, vol. 17, no. 7, pp. 1263–1270, 2000.
- [45] C. S. Goldenstein, V. A. Miller, R. Mitchell Spearrin, and C. L. Strand, “SpectraPlot.com: Integrated spectroscopic modeling of atomic and molecular gases,” *J. Quant. Spectrosc. Radiat. Transf.*, vol. 200, pp. 249–257, 2017.
- [46] F. Riehle, *Frequency Standards*. Wiley-VCH Verlag, 2003.
- [47] J.-H. Lee *et al.*, “III-V/Si Hybrid Laser Stabilization Using Micro-Ring Feedback Control,” *IEEE Photonics J.*, vol. 8, no. 5, 1503507, 2016.
- [48] M. Happach *et al.*, “Temperature-Tolerant Wavelength-Setting and -Stabilization in a Polymer-Based Tunable DBR Laser,” *J. Light. Technol.*, vol. 35, no. 10, pp. 1797–1802, 2017.
- [49] J. P. Epping *et al.*, “Ultra-low-power stress-optics modulator for microwave photonics,” in *Proc. SPIE, Integrated Optics: Devices, Materials, and Technologies XXI*, 10106F, 2017.
- [50] M. Burla *et al.*, “500 GHz plasmonic Mach-Zehnder modulator enabling sub-THz microwave photonics,” *APL Photonics*, vol. 4, no. 5, 056106, 2019.

7 List of publications

Journal articles

- **A. van Rees**, D. Geskus, E.J. Klein, Y. Fan, P. J. M. van der Slot and K.-J. Boller, “Continuous wavelength tuning of an integrated extended-cavity laser beyond its mode spacing limit”, *in preparation*, 2019.
- J. Mak, **A. van Rees**, Y. Fan, E. J. Klein, D. Geskus, P. J. M. van der Slot and K.-J. Boller, “Linewidth narrowing via low-loss dielectric waveguide feedback circuits in hybrid integrated frequency comb lasers,” *Opt. Express*, vol. 27, no. 9, pp. 13307-13318, 2019.

Conference proceedings

- **A. van Rees**, D. Geskus, E. J. Klein, Y. Fan, P. J. M. van der Slot, and K.-J. Boller, “Mode-hop-free Tuning of a Chip-based Hybrid Integrated InP-Si₃N₄ Laser,” in *CLEO/Europe-EQEC, CB-3.5*, 2019.
- J. Mak, **A. van Rees**, Y. Fan, E. J. Klein, D. Geskus, P. J. M. van der Slot and K.-J. Boller, “Narrow Intrinsic Linewidth Frequency Combs from a Chip-Based Hybrid Integrated InP-Si₃N₄ Diode Laser,” in *Conference on Lasers and Electro-Optics*, STu4N.4, 2019.
- Y. Fan, J. Mak, **A. van Rees**, E. J. Klein, and K.-J. Boller, “Extended-Cavity Single-Frequency Semiconductor Lasers using Ring Filters in Low-Loss SiN Technology,” in *IEEE International Semiconductor Laser Conference*, pp. 25-26, 2018.

Oral presentation

- **A. van Rees**, “Tuning of a Hybrid Semiconductor-Glass Waveguide Laser,” in *Applied NanoPhotonics Annual Retreat, Bad Bentheim*, 2018.

Poster presentations

- **A. van Rees**, E. J. Klein, D. Geskus, Y. Fan, and K.-J. Boller, “Mode-hop-free tuning of a chip-based InP-Si₃N₄ hybrid laser,” in *FOM Physics@Veldhoven*, 2019.
- J. Mak, Y. Fan, **A. van Rees**, P. J. M. van der Slot, and K.-J. Boller, “Narrow-linewidth integrated hybrid InP-Si₃N₄ dual-wavelength laser,” in *FOM Physics@Veldhoven*, 2019.
- **A. van Rees**, R. A. M. van Zon, J. Mak, Y. Fan, H. Zia, H. M. J. Bastiaens, D. A. I. Marpaung, P. J. M. van der Slot, C. Fallnich and K.-J. Boller, “Advanced Integrated Light Sources,” in *MESA+ Annual Meeting*, 2018.
- **A. van Rees**, E. J. Klein, D. Geskus, Y. Fan, and K.-J. Boller, “Mode-hop free tuning of a hybrid glass-semiconductor laser,” in *NNV-AMO Lunteren*, 2018.
- J. Mak, Y. Fan, **A. van Rees**, E. J. Klein, D. Geskus, P. J. M. van der Slot and K.-J. Boller, “Narrow-linewidth frequency combs using hybrid semiconductor-glass waveguide lasers,” in *NNV-AMO Lunteren*, 2018.

Appendix A

A.1 Laser cavity free spectral range

To derive the laser cavity free spectral range, we start with Eq. 2.8, which relates the laser cavity roundtrip phase $\theta_{rt,c}$ with the vacuum wavelength λ

$$\theta_{rt,c} = \frac{4\pi L_{eff,c}(\lambda)n_{eff}(\lambda)}{\lambda}, \quad (A.1)$$

where $L_{eff,c}(\lambda)$ is the effective cavity length and $n_{eff}(\lambda)$ is effective refractive index of the dielectric waveguide transverse mode. The effective cavity length depends on the wavelength as both the effective refractive index of the modes and the effective length of the microring resonators are dependent on the wavelength. Within the broad gain bandwidth of the semiconductor amplifier, laser oscillation can occur only at a discrete set of wavelengths that fulfill the resonance condition specified in Eq. 2.3. Combining Eqs. A.1 and 2.3 leads to

$$\frac{2L_{eff,c}(\lambda)n_{eff}(\lambda)}{\lambda} = m_c. \quad (A.2)$$

If we consider the difference of this expression between two consecutive resonant wavelengths, λ_m and λ_{m+1} , with $\lambda_m > \lambda_{m+1}$, the corresponding phases will be $\theta_{rt,c,m}$ and $\theta_{rt,c,m+1}$, respectively. We then obtain

$$\frac{2L_{eff,c}(\lambda_{m+1})n_{eff}(\lambda_{m+1})}{\lambda_{m+1}} - \frac{2L_{eff,c}(\lambda_m)n_{eff}(\lambda_m)}{\lambda_m} \equiv \Delta m_c \left(\frac{2L_{eff,c}(\lambda)n_{eff}(\lambda)}{\lambda} \right) = 1, \quad (A.3)$$

In absence of any spectral filtering, a typical laser cavity has closely spaced longitudinal modes, so that we may approximate Eq. A.3 by

$$1 = \Delta m_c \left(\frac{2L_{eff,c}(\lambda)n_{eff}(\lambda)}{\lambda} \right) \approx -2 \frac{d}{d\lambda} \left(\frac{L_{eff,c}(\lambda)n_{eff}(\lambda)}{\lambda} \right) \Big|_{\lambda=\lambda_m} \Delta\lambda_c, \quad (A.4)$$

where $\Delta\lambda_c \equiv \lambda_m - \lambda_{m+1}$ is called the free spectral range of the laser cavity. For convenience and to easily associate λ_m as a resonant wavelength of the laser cavity, we write as $\lambda_m = \lambda_c$. Note that the product $L_{eff,c}(\lambda)n_{eff}(\lambda)$ appearing in Eq. A.4 contains two effective refractive indices (see Eq. 2.7). For the SOA section of $L_{eff,c}(\lambda)$ the derivative in Eq. A.4 evaluates to

$$-L_{SOA} \frac{d}{d\lambda} \left(\frac{n_{eff,SOA}(\lambda)}{\lambda} \right) \Big|_{\lambda=\lambda_c} \Delta\lambda_c = \frac{1}{\lambda_c^2} L_{SOA} \left(n_{eff,SOA}(\lambda_c) - \lambda_c \frac{dn_{eff,SOA}(\lambda)}{d\lambda} \Big|_{\lambda=\lambda_c} \right) \Delta\lambda_c. \quad (A.5)$$

Using the definition of the group index (Eq. 2.2), Eq. A.5 can be rewritten as

$$-L_{SOA} \frac{d}{d\lambda} \left(\frac{n_{eff,SOA}(\lambda)}{\lambda} \right) \Big|_{\lambda=\lambda_c} \Delta\lambda_c = n_{g,SOA}(\lambda_c) L_{SOA} \frac{\Delta\lambda_c}{\lambda_c^2}. \quad (A.6)$$

A similar expression can be derived for the bus section of the Si_3N_4 waveguides. However, for the Si_3N_4 microrings the effective ring length is also wavelength dependent, leading to extra terms such as $\frac{2\pi n_{eff,Si_3N_4}(\lambda_c)}{\lambda_c} \frac{\partial L_{eff,r1}(\lambda)}{\partial \lambda} \Big|_{\lambda=\lambda_c}$ in the expression for the derivative in Eq. A.4. As we are interested in

mode-hop-free tuning, the resonant wavelength of the resonator must also correspond to resonances of both microring resonators. In Fig. 2.2 it is shown that at resonance, the effective length remains stationary with respect to small variations in the wavelength around the resonant value, so

$\frac{\partial L_{eff,r1}(\lambda)}{\partial \lambda} \Big|_{\lambda=\lambda_c}$ is zero at resonances of the ring and it can be neglected in the evaluation of the

derivative in Eq. A.4. Hence, we obtain

$$1 = -2 \frac{d}{d\lambda} \left(\frac{L_{\text{eff},c}(\lambda) n_{\text{eff}}(\lambda)}{\lambda} \right) \Big|_{\lambda=\lambda_c} \Delta\lambda_c = 2n_g(\lambda_c) L'_{\text{eff},c} \frac{\Delta\lambda_c}{\lambda_c^2}, \quad (\text{A.7})$$

where $L'_{\text{eff},c}$ is the same as Eq. 2.7 but with the ratio $\frac{n_{\text{eff,SOA}}}{n_{\text{eff,Si}_3\text{N}_4}}$ replaced by $\frac{n_{g,\text{SOA}}}{n_{g,\text{Si}_3\text{N}_4}}$ and $n_{g,\text{Si}_3\text{N}_4} \equiv n_g$.

Rearranging Eq. A.7 gives the expression for the FSR of the laser cavity,

$$\Delta\lambda_c = \frac{\lambda_c^2}{2n_g(\lambda_c) L'_{\text{eff},c}}. \quad (\text{A.8})$$

A.2 Laser cavity resonant wavelength tuning

Tuning of the cavity resonant wavelength by including the single pass-phase added by the phase section, ϕ_{ps} , can be modeled, starting from Eq. 2.10,

$$\theta_{\text{rt},c} = \frac{4\pi L_{\text{eff},c}(\lambda_c) n_{\text{eff}}(\lambda_c)}{\lambda_c} + 2\phi_{\text{ps}}, \quad (\text{A.9})$$

where the factor 2 is due to the fact that the light passes the phase section twice during one laser cavity roundtrip. Combining this with the resonance condition (Eq. 2.3) leads to:

$$\phi_{\text{ps}} = m_c \pi - \frac{2\pi L_{\text{eff},c}(\lambda_c) n_{\text{eff}}(\lambda_c)}{\lambda_c}. \quad (\text{A.10})$$

For obtaining $\frac{\partial \lambda_c}{\partial \phi_{\text{ps}}}$ from Eq. A.10, we proceed, for simplification, by determining the inverse expression, $\frac{\partial \phi_{\text{ps}}}{\partial \lambda_c}$,

$$\frac{\partial \phi_{\text{ps}}}{\partial \lambda_c} = \frac{\partial}{\partial \lambda_c} (m_c \pi) - \frac{\partial}{\partial \lambda} \left(\frac{2\pi L_{\text{eff},c}(\lambda) n_{\text{eff}}(\lambda)}{\lambda} \right) \Big|_{\lambda=\lambda_c}. \quad (\text{A.11})$$

To derive the condition for continuous tuning, *i.e.*, that no mode hop occurs, we evaluate Eq. A.11 with the boundary condition that the order of the oscillating mode, m_c , remains constant during tuning, *i.e.*,

$$\frac{\partial}{\partial \lambda_c} (m_c \pi) = 0. \quad (\text{A.12})$$

This condition is only valid if the cavity mode does not hop to a neighboring mode with order $m_c + 1$ (or $m_c - 1$) during tuning of the laser, also called mode-hop-free tuning. By applying Eq. A.12 to Eq. A.11 and using Eq. A.7, we obtain

$$\frac{\partial \phi_{\text{ps}}}{\partial \lambda_c} = -2\pi n_g(\lambda_c) \frac{L'_{\text{eff},c}}{\lambda_c^2}. \quad (\text{A.13})$$

Taking the reciprocal, we obtain

$$\frac{\partial \lambda_c}{\partial \phi_{\text{ps}}} = \frac{\lambda_c^2}{2\pi n_g(\lambda_c) L'_{\text{eff},c}(\lambda_c)} \quad (\text{A.14})$$

Combining Eqs. A.8 and A.14 gives

$$\frac{\partial \lambda_c}{\partial \phi_{\text{ps}}} = \frac{\Delta\lambda_c}{\pi} \quad (\text{A.15})$$

under the condition of mode-hop-free tuning, imposed by Eq. A.12.

A.3 Microring resonator effective length

To derive the effective length of the microring resonator in the laser cavity, we start with the increase in optical phase of the light leaving the drop port of a ring resonator θ_d with respect to the light incident on the input port. This corresponds to an effective geometric propagation length $L_{\text{eff},r}(\lambda_c)$ inside the ring given by Eq. 2.16

$$\theta_d(\lambda_c) = \beta L_{\text{eff},r}(\lambda_c) = \frac{2\pi n_{\text{eff}}(\lambda_c) L_{\text{eff},r}(\lambda_c)}{\lambda_c}. \quad (\text{A.16})$$

Differentiating Eq. A.16 with respect to the laser wavelength gives

$$\frac{\partial \theta_d}{\partial \lambda_c} = 2\pi \frac{n_g(\lambda_c)}{\lambda_c^2} L_{\text{eff},r}(\lambda_c) + \frac{2\pi n_{\text{eff}}(\lambda_c)}{\lambda_c} \frac{\partial L_{\text{eff},r}(\lambda_c)}{\partial \lambda_c}, \quad (\text{A.17})$$

where we have again introduced the group index (Eq. 2.2). Similar to the reasoning leading to Eq. A.7, we neglect the second term on the rhs in the remainder. Solving for the effective length for a longitudinal laser mode gives

$$L_{\text{eff},r}(\lambda_c) \approx \frac{\lambda_c^2}{2\pi n_g(\lambda_c)} \frac{\partial \theta_d}{\partial \lambda_c} \quad (\text{A.18})$$

By applying the chain rule we get

$$\frac{\partial \theta_d}{\partial \lambda_c} = \frac{\partial \theta_d}{\partial \theta_{\text{rt},r}} \frac{\partial \theta_{\text{rt},r}}{\partial \lambda_r} \frac{\partial \lambda_r}{\partial \lambda_c}. \quad (\text{A.19})$$

To avoid mode-hops during tuning of the laser wavelength, it is required that mode-hops are absent in both the laser cavity and in the ring resonator. This is why tuning the laser wavelength requires to tune the resonant wavelength of the laser cavity, λ_c , by the same amount as the resonant wavelength of the ring resonator, λ_r . We call this synchronous tuning, expressed as

$$\frac{\partial \lambda_r}{\partial \lambda_c} = 1. \quad (\text{A.20})$$

In section 2.6 we show how synchronous tuning can be realized by appropriate and synchronous tuning of the phase section and ring resonators. Inserting the condition of synchronous tuning, Eq. A.20, into Eq. A.19, gives

$$\frac{\partial \theta_d}{\partial \lambda_c} = \frac{\partial \theta_d}{\partial \theta_{\text{rt},r}} \frac{\partial \theta_{\text{rt},r}}{\partial \lambda_r}, \quad (\text{A.21})$$

Substituting Eq. A.21 into Eq. A.18 and using Eqs. 2.13 and 2.15 gives

$$L_{\text{eff},r}(\lambda_c) \approx L_{\text{rt},r} \frac{\partial \theta_d}{\partial \theta_{\text{rt},r}}, \quad (\text{A.22})$$

In order to derive an expression for the RHS of Eq. A.22, we use the relation between the input electric field E_{in} of the light and the electric field E_d of the light at the drop given by^[33]

$$E_d = \frac{-\kappa^2 e^{\frac{1}{2}j\theta_{\text{rt},r}}}{1 - t^2 e^{j\theta_{\text{rt},r}}} E_{\text{in}} \quad (\text{A.23})$$

where we have ignored the propagation loss inside the ring resonator, and assumed that both couplers are identical and symmetric, *i.e.*, $\kappa_1 = \kappa_2 \equiv i\kappa$ and $t_1 = t_2 \equiv t$ with both κ and t real quantities. Ignoring the propagation loss is a reasonable assumption for the low-loss Si_3N_4 waveguide platform we are considering here. Rewriting Eq. A.23 gives

$$E_d = \frac{-\kappa^2}{e^{-\frac{1}{2}j\theta_{\text{rt},r}} - t^2 e^{\frac{1}{2}j\theta_{\text{rt},r}}} E_{\text{in}}. \quad (\text{A.24})$$

On the other hand,

$$E_d = |E_d|e^{j(\theta_d + \theta_{in})}, \quad (\text{A.25})$$

where θ_{in} is the optical phase of the light at the input port of the ring resonator. Comparing Eq. A.25 with Eq. A.24 shows that the optical phase advance of the light from input port to drop port is given by

$$\theta_d = \text{Arg} \left(\frac{-\kappa^2}{e^{-\frac{1}{2}j\theta_{rt,r} - t^2} e^{\frac{1}{2}j\theta_{rt,r}}} \right). \quad (\text{A.26})$$

As laser oscillation will take place near the peak of the resonance, where feedback of the light into the gain medium is strong, *i.e.*, the roundtrip losses of the laser cavity are small, we can find an analytic expression for the effective length of the resonator, $L_{\text{eff},r}(\lambda)$ under the condition of near resonance operation. We therefore write $\theta_{rt,r} = \theta_n + \delta\theta_{rt,r} = n2\pi + \delta\theta_{rt,r}$, where $\delta\theta_{rt,r}$ remains small ($|\delta\theta_{rt,r}| \ll 1$). Using this assumption, we can rewrite Eq. A.26 as

$$\theta_d = \text{Arg} \left(\frac{-\kappa^2}{(-1)^n \left[e^{-\frac{1}{2}j\delta\theta_{rt,r} - t^2} e^{\frac{1}{2}j\delta\theta_{rt,r}} \right]} \right). \quad (\text{A.27})$$

As $|\delta\theta_{rt,r}| \ll 1$, we can use $e^{\pm\frac{1}{2}j\delta\theta_{rt,r}} \approx 1 \pm \frac{1}{2}j\delta\theta_{rt,r}$ and substitute this in Eq. A.27 to obtain

$$\theta_d = \text{Arg} \left(\frac{-\kappa^2}{(-1)^n \left[(1 - \frac{1}{2}j\delta\theta_{rt,r}) - t^2 (1 + \frac{1}{2}j\delta\theta_{rt,r}) \right]} \right). \quad (\text{A.28})$$

Equation A.28 can be written as

$$\theta_d = \text{Arg}(-\kappa^2) - \text{Arg}((-1)^n) - \text{Arg} \left(1 - t^2 - \frac{1}{2}j\delta\theta_{rt,r}(1 + t^2) \right), \quad (\text{A.29})$$

and evaluating yields

$$\theta_d = (1 - n)\pi - \text{Arg} \left(1 - t^2 - \frac{1}{2}j\delta\theta_{rt,r}(1 + t^2) \right). \quad (\text{A.30})$$

We are interested in the phase added to the optical field by the ring resonator when reaching the drop port, close to resonance, so we rewrite Eq. A.30 in the form of $\theta_d = (1 - n)\pi + \delta\theta_d$ to obtain

$$\delta\theta_d = -\text{Arg} \left(1 - t^2 - \frac{1}{2}j\delta\theta_{rt,r}(1 + t^2) \right). \quad (\text{A.31})$$

By rewriting the argument on the r.h.s. of Eq. A.31 in the form of $z = x + jy$ and using $\tan(\text{Arg}(z)) = \frac{y}{x}$ we get

$$\tan(\delta\theta_d) = \frac{1+t^2}{2(1-t^2)} \delta\theta_{rt,r}. \quad (\text{A.32})$$

Since $|\delta\theta_{rt,r}| \ll 1$, the rhs of Eq. A.32 is small and we may approximate $\tan(\delta\theta_d) \approx \delta\theta_d$ and

$$\delta\theta_d \approx \frac{1+t^2}{2(1-t^2)} \delta\theta_{rt,r}. \quad (\text{A.33})$$

Since $\kappa^2 + t^2 = 1$ for a loss-free coupler, this can be written as

$$\delta\theta_d \approx \left(\frac{1}{2} + \frac{1-\kappa^2}{\kappa^2} \right) \delta\theta_{rt,r}. \quad (\text{A.34})$$

Equation A.34 shows that near resonance the phase advance at the drop port, and hence the effective length of the ring resonator is significantly enhanced when the ring has a small coupling to the bus waveguide. Combining Eqs. A.22 with A.34 we obtain an expression of the effective microring resonator length, under condition of near resonance operation,

$$L_{\text{eff},r} \approx L_{\text{rt},r} \left(\frac{1}{2} + \frac{1-\kappa^2}{\kappa^2} \right). \quad (\text{A.35})$$

Equation A.35 shows that $L_{\text{eff},r}$ is independent of the resonant wavelength as long as the coupling constant κ is independent of the wavelength.